Structural inheritance and border fault reactivation during active early-stage rifting along the Thyolo fault, Malawi

Luke N. J. Wedmore[1], Jack N Williams[2], Juliet Biggs[1], Åke Fagereng[2], Felix Mphepo[3], Zuze Dulanya[4], James Willoughby[1], Hassan Mdala[3], Byron Adams[1]*

[1]*School of Earth Sciences, University of Bristol, UK*

[2]*School of Earth and Ocean Sciences, Cardiff University, UK*

[3]*Geological Survey Department, Mzuzu Regional Office, Mzuzu, Malawi*

[4]*Geography and Earth Sciences Department, University of Malawi, Zomba, Malawi*

**Corresponding author: luke.wedmore@bristol.ac.uk*

Keywords

High-resolution topography, pre-existing structures, normal faults, rifts, border fault, damage zone

Highlights

- The Thyolo fault, Malawi, is a rift border fault with a polyphase tectonic history
- Satellite and field data confirm recent activity on an 18.6 ± 7.7 m high scarp
- The fault is segmented, but scarp height minima do not align with geometry changes
- Pre-existing shallow structures control the surface geometry and 0.7 m wide fault core
- Fault displacement is affected by viscous reactivation along a terrane boundary

Abstract

We present new insights on the geometry, initiation and growth of the Thyolo fault, an 85 km long active border fault in the southern Malawi Rift, from high-resolution topography, field and microstructural observations. The Thyolo fault is located towards the edge of the Proterozoic Unango Terrane, and is the border fault of the Lower Shire Graben, which has experienced four phases of extension since the Jurassic. Recent activity is demonstrated by an 18.6 ± 7.7 m high fault scarp, with two substantial reductions in scarp height along strike. However, the segment boundaries suggested by these displacement measurements do not coincide with changes in fault strike. Elsewhere, a ~5 km long fault perpendicular scarp joins two overlapping sections, yet the scarp height in this linking section is similar to the bounding sections, and there is no evidence of significant pre-linkage strain accumulation. Microstructural analyses along the fault show a 15-45 m thick footwall damage zone with a 0.7 m thick core. We suggest that favourably-oriented, pre-existing shallow structures control changes in surface geometry and the narrow fault core, whereas exploitation of weak ductile zones at depth, possibly associated with the terrane boundary, control the displacement profile of the fault.

1. Introduction

Narrow amagmatic rifts (sensu Buck, 1991) are typically characterised by a ≤100 km wide graben or half graben where the greatest cumulative displacement is accommodated on large offset normal fault systems, known as rift border faults, that bound a region of distributed but relatively small displacement brittle deformation (Ebinger, 1989; Gawthorpe and Leeder, 2000; Muirhead et al., 2019). These basin-bounding faults are thought to be most active prior to any magmatic influence on rifting (Ebinger, 2005; Muirhead et al., 2019), have a distinctive impact on basin geomorphology (Leeder and Gawthorpe, 1987; Gawthorpe and Leeder, 2000) and can accumulate sufficient displacement to induce flexural bending within the hanging wall basin (Turcotte and Schubert, 2002). Border faults can penetrate the entire depth of the crust, and in East Africa are probably the source of some of the deep earthquakes that occur within the 30-40 km thick seismogenic layer (Jackson and Blenkinsop, 1993; Craig et al., 2011; Lavayssière et al., 2019).

How faults grow from nucleation to crustal scale features is a long-standing topic of research (Cowie and Scholz, 1992b; Cowie, 1998; Walsh et al., 2002; Nicol et al., 2005; Worthington and Walsh, 2017; Rotevatn et al., 2019), and numerous studies have mapped fault trace geometry and measured displacement-length profiles to discuss the mechanism and timing of how long faults develop through segment initiation, growth, and linkage (Cowie and Scholz, 1992a, 1992b, 1992c; Scholz et al., 1993; Dawers et al., 1993; Dawers and Anders, 1995; Schlische et al., 1996; Walsh et al., 2003; Nicol et al., 2005, 2017; Giba et al., 2012; Rotevatn et al., 2018). Structural heterogeneities at segment boundaries, such as fault bends and step-overs, are thought to influence the propagation and termination of earthquake ruptures (Segall and Pollard, 1980; Zhang et al., 1991; Wesnousky, 2006, 2008). However, recent earthquakes (e.g. 2010 M_w7.2 El Mayor-Cucapah Earthquake, Mexico – Wei et al., 2011 and the 2016 M_w7.8 Kaikoura Earthquake, New Zealand – Hamling et al., 2017) have propagated across multiple segment boundaries, making it unclear how to best assess fault segmentation for seismic hazard purposes (DuRoss et al., 2016). Border faults are now generally thought to develop through the accumulation of displacement on fault segments that formed and linked during the early stages of rifting (Gawthorpe et al., 2003; Rotevatn et al., 2019; Muirhead et al., 2019); however, the effects of this linkage on the displacement profile and surface trace of a fault are commonly long-lasting (McLeod et al., 2008). Minima in fault displacement profiles are persistently observed at segment boundaries

(Machette et al., 1991; Gupta and Scholz, 2000; Mortimer et al., 2007, 2016) as are relay ramps, increased fault complexity, step-overs, and changes in fault orientation (Leeder and Gawthorpe, 1987; Crone and Haller, 1991a; Peacock and Sanderson, 1991; Crider and Pollard, 1998; McLeod et al., 2008; Fossen and Rotevatn, 2016; Hodge et al., 2018a). Thus, observations of fault segmentation provide a permanent record of processes that occurred during the formation and linkage of fault segments, and consequently they offer insights into the fundamental processes of fault growth and the controls on the limits of earthquake rupture propagation.

Rifts rarely initiate and grow in isotropic crust, and therefore it is important to understand the effect of pre-existing heterogeneities and structures on the growth and segmentation of faults. These pre-existing structures are often cited as the predominant control on rift geometry, the distribution of strain within rifts, and the orientation of magmatic bodies, magmatic rift segments and faults within rifts (McConnell, 1967; Daly et al., 1989; Ebinger et al., 1997; Morley, 2010; Henstra et al., 2015; Robertson et al., 2016; Muirhead and Kattenhorn, 2018). At the scale of an individual fault, analogue models have shown that reactivation of pre-existing fabrics affects fault growth by influencing fault orientation, relay zone geometry and the distribution of basins (Bellahsen and Daniel, 2005; Henza et al., 2011). However, comparisons of these models with natural faults is challenging as it can be difficult to differentiate between contemporary and pre-rift heterogeneities that have similar geometries (Smith and Mosley, 1993; Holdsworth et al., 1997), especially using seismic reflection and aeromagnetic surveys, which can only resolve features at scales >10 m.

Investigating the interactions between pre-existing fabrics and strain localisation on rift border faults also requires understanding the structure and mechanics of these faults. In general, as faults grow, the rocks surrounding the fault accumulate damage (Cowie and Scholz, 1992b; Caine et al., 1996; Shipton and Cowie, 2003). However, the structure of a rift border fault has only been described in a limited number of cases (Ord et al., 1988; Wheeler and Karson, 1989; Kristensen et al., 2016; Hollinsworth et al., 2019), with most models of normal fault structural evolution based on studies of small displacement (<100 m) faults within high porosity sedimentary rock (Shipton and Cowie, 2003; Childs et al., 2009; Torabi and Berg, 2011; Savage and Brodsky, 2011). Consequently, it remains unclear whether these models are applicable to large offset rift border faults where the footwall is composed of foliated crystalline metamorphic rocks.

In this paper, we analyse the Thyolo fault, the border fault of the Lower Shire Graben in southern Malawi (Figure 1). The fault is an ideal location to study the effects of pre-existing structures on fault geometry and structure as the graben has a well-documented polyphase history of extension (Castaing, 1991; Chisenga et al., 2019). Furthermore, thin syn-rift sediments mean that fault exposures formed during the current rift phase are not hidden by post-rift sediments (e.g. Hodge et al., 2019; Williams et al., 2019). We begin by describing the tectonic history of the region, before analysing the current activity, geometry and structure of the fault. In doing so, we assess how reactivation of pre-existing fabrics and heterogeneities at different scales affects the evolution of a rift border fault.

2. Tectonic History

The Thyolo fault bounds the north-eastern edge of the Lower Shire Graben, which is located at the southern end of the largely amagmatic Western branch of the East African Rift (EAR; Figure 1). Extension within the Western branch of the EAR initiated ~25 Ma (Roberts et al., 2012) and within southern Malawi, the current horizontal geodetic extension rate is ~2 mm yr^{-1} (relative to the stable Nubian plate; Stamps et al., 2018; Figure 1). It is not known whether this extension rate has been constant during the current phase of rifting (the last ~25 Ma).

The footwall of the Thyolo fault is composed of charnockitic gneiss and granitic granulites of the Mesoproterozoic Unango Terrane, part of the Mozambique Belt, with the fault located towards the southwestern edge of the terrane (Figure 2; Fullgraf et al. *in press*; Bloomfield, 1965; Johnson et al., 2005). The Unango Terrane likely formed in a continental volcanic arc setting at ~1 Ga, and experienced granulite facies metamorphism associated with ductile deformation shortly after emplacement (957 ± 27 Ma; Bingen et al., 2009). The metamorphic foliation and migmatitic banding in the Thyolo fault's footwall dips moderately SW. The foliation formed at granulite facies metamorphic conditions coincident with partial melting during a series of collisional events at a convergent continental margin in the Pan-African Orogeny (~710-555 Ma) associated with the amalgamation of Gondwana (Kröner et al., 2001; Johnson et al., 2005; Manda et al., 2019). In the region of the Thyolo fault, the edge of the Unango Terrane is in contact with the basement of the South Irumide Belt, which underwent peak metamorphism between 1.06 and 1.05 Ga (Johnson et al., 2005; Westerhof et al., 2008; Karmakar and Schenk, 2016). The terrane boundaries have been roughly mapped based on exposures within Malawi (Manda et al., 2019), but because younger cover sequences (~330-180 Ma Karoo-age sedimentary rocks) have obscured the basement, the unit boundaries are largely extrapolated from neighbouring Mozambique, where mapping was supported by geochemical and airborne magnetic data (Bingen et al., 2009; Macey et al., 2010).

2.1 Previous phases of rifting

The Lower Shire Graben contains Phanerozoic sedimentary and volcanic deposits related to three regional phases of extension that occurred prior to the current rifting (i.e. prior to ~25 Ma): two distinct events during the Karoo-age breakup of Gondwana (~330-180 Ma), and a later phase at the end of the Jurassic and into the early Cretaceous (~140-110 Ma; Castaing, 1991; Figure 2).

NW-SE Karoo-age transtension in the Lower Shire Graben created space to deposit a sequence of Late Ecca (Middle Permian) to Late Beaufort (Early Triassic) coal shales, coarse grained grits, mudstones and sandstones (orange units in Figure 2c). These sedimentary rocks are bound by E-W striking normal faults and NW-SE striking dextral strike-slip faults including the Mwanza and possibly the Thyolo fault (Figure 2c; Habgood, 1963; Habgood et al., 1973; Castaing, 1991).

NW-SE extension continued into the late Karoo period, when it was associated with basaltic volcanism and contemporaneous emplacement of NE-SW striking dolerite dykes. These dykes and volcanic deposits are collectively known as the Stormberg Volcanics, which are widely observed in the footwalls of the Mwanza, Thyolo and Mtumba faults (Figure 2d; Habgood, 1963; Habgood et al., 1973; Woolley et al., 1979; Castaing, 1991).

After the Karoo period, during the Late Jurassic – Cretaceous, the extension direction rotated from NW-SE to NE-SW and reactivated NW-SE structures established in the earlier phase of NW-SE transtension as dip-slip normal faults (Figure 2e; Castaing, 1991). In the Lower Shire Graben, remnant deposits from the NE-SW extension are limited to sandstones in the hanging wall of the Panga and Chitsumba faults (Figure 2e) and siliceous fault rock along the Namalambo Fault (Habgood, 1963; Habgood et al., 1973). These sedimentary deposits form part of the Lupata series, a mix of coarse grained sandstones, and rhyolitic and alkaline lavas found extensively in Mozambique (Dixey and Campbell Smith, 1929; Habgood, 1963), and were emplaced contemporaneously with the Chilwa Alkaline Province, which involves intrusive rocks that crosscut the Stormberg dykes (Macdonald et al., 1983; Woolley, 1987; Castaing, 1991; Eby et al., 1995). Cretaceous activity on the Thyolo and/or Mwanza faults cannot be ruled out as current syn-rift sediments will likely have buried any Cretaceous sedimentary deposits.

2.2 Current rifting

Previous studies have interpreted the Thyolo fault as an active, reactivated dextral strike-slip fault linking the Urema Graben (the southern active continuation of the EARS in Mozambique) and the Zomba Graben (Castaing, 1991; Chorowicz and Sorlien, 1992; Chorowicz, 2005). In other studies, the Thyolo fault is considered inactive (Laõ-Dávila et al., 2015; Prater et al., 2016). Hodge et al. (2019) combined remote sensing observations with field observations to show that the fault is active, by documenting a pseudo-continuous fault scarp and triangular facets at the southern end of the fault. However, the fault was divided into two separate faults, the Thyolo and Muona faults, based on the separation distance between their scarps

(Hodge et al., 2019). A M_w5.6 earthquake in March 2018 had a normal faulting focal mechanism with nodal planes aligned with the surface traces of faults in the Lower Shire Graben (Figure 1; Ekström et al., 2012). Williams et al. (2019) suggest that the Thyolo fault is currently active as a dip-slip normal fault oriented obliquely to the ENE-WSW regional extension direction. Below, we describe in detail the dimensions and geometry of the fault scarp, and the fault damage zone along the Thyolo fault, and analyse the factors that control fault segmentation, orientation and structure.

3. Methodology

3.1 Fault segmentation analysis

We used a high resolution 12 m TanDEM-X digital elevation model (DEM) to identify different indicators of fault segmentation based on two distinct sets of criteria: map-view geometry and scarp height. We mapped the fault trace in high resolution and noted prominent changes in fault strike, map-view fault steps, fault branches, increased fault complexity or gaps, which are considered geometrical indicators of fault segmentation (Zhang et al., 1991; Wesnousky, 2008; DuRoss et al., 2016).

Fault segmentation can also be defined from the along-fault displacement profile (e.g. Dawers and Anders, 1995; Willemse et al., 1996; Willemse, 1997; Walsh et al., 2003). In a plot of fault displacement vs. fault-parallel distance, the segment boundaries are usually located at local displacement minima (Crone and Haller, 1991a; Dawers and Anders, 1995; Walsh et al., 2003). We used scarp height as a proxy for displacement (e.g. Morewood and Roberts, 2000; Hodge et al., 2018b, 2019; Wedmore et al., 2020) and identified segments based on local minima in the along-strike scarp height profile. We used adapted versions of the SPARTA scarp measuring tools (Hodge et al., 2019) to measure the height of the fault scarp along the Thyolo fault on the 12 m DEM. We differ from Hodge et al. (2019) by extracting 500 m long fault-perpendicular topographic profiles from the DEM every 12 m along the fault, which were averaged by stacking at 100 m intervals before measuring the vertical difference between regression lines on the footwall and hanging wall surfaces. We estimated the uncertainty of each measurement by applying a Monte Carlo approach to sample 10,000 random subsets of points from the hanging wall and footwall of the fault as well as allowing the location of the fault to vary along the section of the topographic profiles identified as the fault scarp. The resulting measurements of vertical offset were then filtered using a 5 km wide moving median filter along the strike of the fault.

We also examined the Thyolo fault for any evidence of features associated with fault linkage. Where two un-linked fault segments interact, fractures and faults form such that the faults maintain laterally constant extensional strain (Walsh and Watterson, 1991). These features create relay zones or transfer structures, which evolve as the faults overlap and link. Typically relay structures have 10-15° dipping ramps and breach structures that link the segments (Fossen and Rotevatn, 2016). Before a linking fault has breached a relay ramp, propagating and overlapping fault tips induces rotation (about a vertical axis) within the transfer structure (Fossen and Rotevatn, 2016). To identify linking structures, we analysed variations in the strike of the fault by dividing the fault trace into 50 m long sections and measuring the strike of each section from the trend of the surface trace, assuming negligible topography. The orientation of pre-existing basement structures were analysed by digitising the

3D foliation measurements and strike of dolerite (Stormberg) dykes in Habgood et al. (1973).

The fault scarp and geometry of some of the structures that we observed in the remote sensing data and geological maps were ground-truthed during field campaigns in 2017 and 2018, during which additional observations were made regarding the structure and slip sense of the fault.

3.2 Fault zone meso- and microstructural analysis

We made lithological and structural observations of the footwall damage zone of the Thyolo fault along four transects, Kalulu, Kanjedza, Mbewe, and Muona (Figure 3), which extended from the fault scarp to distances up to 280 m into the footwall. In addition, we collected samples at Kalulu (n = 5) and Kanjedza (n = 11) for microstructural and compositional analyses. Individual samples were accurately located using digital elevation models and orthophotos constructed from drone-based photogrammetry, as well as handheld GPS measurements. Sample thin sections were photographed in plane-polarised and cross-polarised light, and fracture density was calculated from manually traced fractures in three 10-15 mm^2 areas in each sample using FracPaQ 2.2 (Healy et al., 2017). We only traced fractures in quartz or feldspar grains, to allow comparison between lithologically diverse samples, and used an area-weighted average as the fracture density value for each thin section (see supplementary text for full details of sample collection, preparation and analysis).

4. Results

4.1 The Thyolo Fault

The Thyolo fault has a recently active fault scarp at the base of a ~1 km high footwall escarpment (Figure 3 & 4). Note that we consider the previously described Thyolo and Muona faults as a singular 'Thyolo fault', rather than two separate structures (in contrast to Hodge et al., 2019) because the Chisumbi link section connects the Thyolo and Muona sections of the fault without a break in the scarp (Figures 3-5 and Section 4.4). Triangular facets are visible within the high-resolution topography along the southeastern end of the Thyolo section and the northwestern end of the Muona section (Figure 3), and were also observed in the field (Figure 4). We observed no systematic deflection of river channels or any other geomorphological features that might indicate strike-slip faulting (Figure S1), and we therefore consider the Thyolo fault to be currently accommodating pure normal dip-slip displacement (see also Williams et al., 2019).

4.2 Map View Geometry

The Thyolo fault is ~85 km long and has a mean strike of 139 ± 15° (1 standard deviation) dipping to the southwest (Figure 3 & 4). A fault scarp is visible in the high-resolution topography along the length of the fault, with gaps observed where ≤ 100 m wide rivers cross the fault and have eroded the scarp (Figure 3b). However, the effect of rivers on the observations in Figure 5 is negligible as we did not measure scarps in these locations, and the final scarp height is averaged over 5 km along strike to smooth short-wavelength features such as these rivers. We find seven sections along the fault trace that trend approximately perpendicular to the average fault strike (Figure 5c). These NE-SW oriented sections have a mean strike of 044 ± 28° (black lines in Figure 5) with five sections dipping to the northwest and two sections dipping to the southeast. The dip angle of these NE-SW oriented sections is unknown but is likely >30° based on the slope of the facet in the escarpment above (Figure 6; Tucker et al., 2011). The most prominent of these NE-SW sections forms a 4.8 km orthogonal link between the Thyolo and Muona sections (Figure 6). The ~69 km long Thyolo and the ~28 km long Muona sections overlap by ~10 km and are connected by this 4.8 km long section, which we refer to as the Chisumbi section. The six other scarp sections that trend perpendicular to the average fault strike are each <500 m long.

The mean strike of the pre-existing metamorphic foliation, within the footwall basement of the Thyolo fault, is 140 ± 37° with a dip of 56 ± 12° SW (Figure 5 & 6). This is subparallel to the mean strike of the fault scarp (139 ± 15°; Figure 5). A fault dip could only be constrained in the field at Kalulu, nevertheless, this measurement (60°) and the range of active normal fault dips elsewhere in Malawi (45°-60°; Hodge et al., 2018b; Kolawole et al., 2018; Williams et al., 2019) and globally (Collettini and Sibson, 2001) suggest that the Thyolo fault dips subparallel to the foliation. Conversely, the mean strike of the dolerite dykes in the fault's footwall (calculated by digitising the orientation of the contact between the dyke and basement rock) is 037 ± 9°, which is within error of the strike-perpendicular sections of the fault (044 ± 28°; including the Chisumbi section). Our field measurements at four localities along the Thyolo Fault indicate that the dykes are subvertical (Figure 3a).

4.3 Scarp Height

The median height of the fault scarp along the Thyolo fault is 18.6 ± 7.7 m (Figure 5). The along-strike profile of the scarp height measurements shows two scarp height minima (besides the fault tips; Figure 5b). The distance from the north-western fault tip to the first minimum is 28 km with a median scarp height of 24.9 ± 9.0 m in this portion of fault (Figure 5b). The middle portion of the fault is 15 km long and has a median scarp height of 20.8 ± 6.3 m. The south-eastern portion is 48 km long with median scarp height of 17.8 ± 6.5 m (Figure 5b). None of the scarp height minima identified from the scarp height profile coincide with changes in fault strike, i.e. the short segments that trend perpendicular to the average fault strike (Figure 5). The scarp height minimum that occurs at ~53 km on Figure 5 is adjacent to a region where the foliation strike varies within a range of ~70° around the mean. The region contains both typical and somewhat anomalous orientations, and although it may be an area of structural complexity, it does not stand out as markedly different from elsewhere along the fault.

4.4 The Chisumbi Section

The 4.8 km Chisumbi section links the Muona and Thyolo sections (Figure 4b) and has a strike of 046 ± 31°, which is approximately orthogonal (93 ± 34°) to the average strike of the main fault (139 ± 15°) but subparallel to the average strike of the dolerite dykes (037 ± 9°; Figure 6). Along this linking section, we observed a 19.0 ± 4.2 m high scarp (median value; see example profile D in Figure 3b; Figure 5). This height (yellow triangle in Figure 5b) is within the error bounds of the scarps found along the adjacent Muona and Thyolo sections. Thus, the fault scarp along Chisumbi section trends approximately perpendicular to the bounding sections, but has a similar scarp height.

Within the footwall of the Chisumbi section, where the Muona and Thyolo sections overlap, the dolerite dykes have a strike of 031 ± 9° whereas the strike of the dolerite dykes outside the overlap zone is 038 ± 9° (Figure 6b). Thus, as these values are within the error bounds of each other, the average trace of dykes within the overlapping zone have either no rotation or a slight anticlockwise rotation around a vertical axis (Figure 6b). The dip of the topography in the footwall of the Chisumbi section (excluding the facet slope above the fault scarp) is 2° (Figure 6c),

4.5 Damage zone and fault core structure of the Thyolo fault

4.5.1 Lithology

The contact between hanging-wall sediments, and footwall gneisses and granulites of the Unango Terrane, is exposed at Kalulu (Figure 7), where these two units are separated by an approximately 60° dipping, 0.7 m thick, incohesive white to minty green fault gouge. The gouge contains a brown clay-rich matrix (70-90% by area) with subangular to subrounded quartzofeldspathic clasts (10-30% by area) up to 3 mm in size (Figures 7b and S2). A 5-15 m thick zone of incohesive quartzofeldspathic granulite and hornblende gneiss borders the fault gouge. At the other three localities where field exposures of the fault were studied, a 15-45 m wide unit of incohesive biotite ± hornblende ± pyroxene gneiss is present adjacent to the scarp, beyond which, the gneiss appears more intact (Figures 8 and S3). The gneissic foliation is defined by alternating quartzofeldspathic and biotite ± hornblende ± garnet bands, in which elongate biotite grains are aligned to and also define a foliation subparallel to the compositional banding. Subvertical, NE-SW striking Stormberg dolerite dykes crosscut the gneisses at all distances from the fault.

4.5.2 Fault zone structure

Quartzofeldspathic clasts within the fault gouge at Kalulu are intensely fractured and sheared (Figure 7), and therefore we interpret this 0.7 m zone as the fault core (sensu Caine et al., 1996). In the incohesive gneisses and granulites in the footwall beyond the fault core, the metamorphic foliation and pegmatite veins are generally preserved (Figure 9 and S4), although locally offset by < 0.6 m along minor faults (i.e. discrete secondary faults within the footwall of the main fault; Figure 8d). At Kanjedza, a 2 m wide ductile reverse shear zone has been exploited by a NW-SE striking dyke whose emplacement predates movement on the Thyolo fault, as it has been offset by a minor normal fault (Figure 8c). At Mbewe, a 50 cm thick, scarp-parallel, steeply dipping foliated fault gouge is present 10 m into the footwall, and juxtaposes charnockite and locally folded hornblende gneisses (Figure S3).

In the incohesive gneisses < 50 m from the Thyolo fault, quartz and feldspar grains exhibit fracture densities of 2.3-4.8 mm^{-1}, with most fractures oblique to the foliation (Figure 9 and Figure S5). These fractures are generally intragranular and closed, but there are rare cases of biotite and calcite mineralisation, which are most prevalent close to minor faults and/or dykes (Figure 9b). Microscale fracture density within the intact gneisses 50-280 m from the Thyolo fault is 0.9-2.2 mm^{-1}, and fractures are almost exclusively parallel to the foliation (Figure 9e). We interpret the 15-45 m wide unit of incohesive gneiss with a relatively high density of foliation-oblique microfractures, but little evidence of shear displacement, as the footwall damage zone (sensu Caine et al., 1996). At distances > 45 m from the fault, the gneiss is intact, and there is no major changes in composition. Therefore, we are confident that the incohesive nature of the damage zone is related to brittle deformation and fracturing around the fault, and any physical weathering or chemical alteration is enhanced by and linked to fault-related fracture damage.

We do not observe a systematic decay in fracture density with distance from the fault within the 15-45 m wide damage zone of the Thyolo fault (Figure 9). This may reflect damage around minor faults and dykes within the damage zone (e.g. Figure 9b), the lack of consistently oriented samples with respect to the fault, a sample bias that misses the most damaged rocks because they are impossible to sample intact, and/or variations in grain size and composition. The microfracture density increase inside the damage zone relative to the background level is relatively minor (Figure 9g*;* compare with Wilson et al., 2003; Mitchell and Faulkner, 2009). It is difficult to assess if this small increase in fracture density represents a relatively low fracture density in the damage zone, or selective sampling of more cohesive portions of the damage zone for analysis.

5. Discussion

The 18.6 ± 7.7 m fault scarp and triangular facets indicate that the Thyolo fault has been reactivated during the current stage of East African Rifting (since 25 Ma), although the steepness of the scarp indicates that it probably formed in the Late-Quaternary or it would have degraded further (Hodge et al., 2020). Whereas the Thyolo fault is dominantly subparallel to the metamorphic foliation, there are notable sections where the strike turns by ~90˚ and the fault scarp trends subparallel to the strike of Stormberg-age subvertical dolerite dykes (Figure 6).

5.1 Fault segmentation

Scarp height minima and changes in surface fault trend are generally considered indicators of fault segment boundaries (Crone and Haller, 1991b; Machette et al., 1991; Peacock and Sanderson, 1991; Crider and Pollard, 1998; Mortimer et al., 2007, 2016; Fossen and Rotevatn, 2016). However, along the Thyolo fault, the locations of scarp height minima do not coincide with changes in the trend of the fault scarp (Figure 5).

The sections that trend perpendicular to the overall strike of the Thyolo fault range in length from 170 m to 4.8 km. Because of our method of measuring strike as a 50 m average, we may have missed < 50 m long strike-perpendicular sections that coincide with the scarp height minima. However, we do not see short fault-perpendicular sections near the scarp height minima on the scarp maps made from the 12 m DEM. Only one of the fault-perpendicular sections (the Chisumbi section) would normally be considered long enough to be a segment boundary based on geometrical criteria (i.e. ≥ ~3-5 km; Wesnousky, 2008). This geometry has been used to argue that the Thyolo and Muona sections are different faults (Hodge et al., 2019). However, a previously unrecognised fault scarp along the Chisumbi section links the Thyolo and Muona sections, and the height of this scarp is in the same range as scarps along the bounding Thyolo and Muona sections (Figure 3b, profile D; Figure 5b). The presence of this continuous scarp implies that during the recent earthquakes that formed the scarp, slip likely propagated along and through the 4.8 km long, ~90° kink in the fault. Given the ~600 m high escarpment and triangular facets along the Chisumbi section it is also likely that slip has persistently propagated along this section over longer geological time, through what would typically be considered geometrical segment boundaries (Figure 10c). Consequently, on faults that have reactivated pre-existing fabrics, purely geometrical criteria for identifying fault segmentation may not adequately identify segment boundaries.

The Chisumbi section lacks evidence for distributed strain in the area between the tips of the Thyolo and Muona sections it links (Figure 10). There is no or minor anticlockwise rotation of dykes in the footwall of the Chisumbi section, and the topographic slope dips at a much shallower angle (~2°; Figure 10) compared to a global study of the dip of breached relay ramps (10-15°; Fossen and Rotevatn, 2016). Although the comparatively gentle ramp dip may be because most examples in the global catalogue are from sedimentary rocks, it remains clear that little strain accumulated within the Chisumbi section prior to the bounding Thyolo and Muona sections becoming linked. The morphology of the Chisumbi linkage section is most similar to a mid-ramp relay zone breach (Figure 10), which appears to be favoured in locations with brittle basement rock and/or where pre-existing structures are reactivated (Fossen and Rotevatn, 2016). When the distance between bounding sections is less than 20% of their total fault length, Hodge et al. (2018a) suggest that breaching occurs as slip is promoted by positive Coulomb stress changes in the linking region. As the ~5 km Chisumbi section is <20% of the ~80 km Thyolo fault, we propose that the Thyolo and Muona sections are linked by weak structures that were activated by Coulomb stress changes in the shallow upper crust. This linkage occurred prior to the accumulation of significant strain within the relay zone, and the link section no longer operates as a permanent barrier to earthquake rupture and propagation (Figure 10d).

5.2 Thyolo fault zone structure

The Thyolo fault has a ~1 km high footwall escarpment, which suggests that the total displacement across the fault is at least 1.2 km (assuming a 60° fault dip) and the damage zone documented here reflects fault-related deformation within a kilometre of the surface. The 15-45 m thick footwall damage zone is within the range of other faults with km-scale displacement in global comparisons, whereas the 0.7 m fault core is relatively narrow (Torabi and Berg, 2011; Savage and Brodsky, 2011; Torabi et al., 2019). However, there is considerable scatter in these global comparisons owing to variations in fault kinematics, lithology and depth of faulting. A more instructive comparison may be to the Dombjerg fault, Greenland, which is another well exposed rift border fault of similar scale to the Thyolo fault (3 km throw, ~100 km long), with a footwall hosted in crystalline metamorphic basement rocks that contain a fault-parallel gneissic foliation. The Dombjerg fault footwall damage zone is 600 m wide, ~10 times wider than the Thyolo fault, and the core comprises several <0.5 m thick strands of gouge and breccia in a ~200 m wide zone, (Kristensen et al., 2016), whereas the single Thyolo fault core is 0.7 m thick. The thicker and more distributed nature of the Dombjerg fault core compared to the Thyolo fault core may reflect that the Dombjerg fault was studied near a step between two fault segments (Kristensen et al., 2016). On the other hand, our observations from the Thyolo fault were taken from sites where there is no obvious geometrical complexity. The smaller fault zone thickness and localised, single fault core in the Thyolo fault support theories where the distribution of fault complexities during initiation and growth control fault zone width (Kim and Sanderson, 2005; Childs et al., 2009). Localised slip and a narrow damage zones are observed for other faults that follow pre-existing discontinuities (Heermance et al., 2003; Zangerl et al., 2006), and so the fault-parallel foliation may have also contributed to the Thyolo fault's relatively narrow structure. Therefore, where a fault such as the Thyolo fault initiates, grows and lengthens rapidly in mechanically anisotropic crust, a narrow damage zone and core initially forms, prior to any increase in damage that may occur with the accumulation of larger displacements (e.g. Kolyokhin and Torabi, 2012).

5.3 Mechanism of fault reactivation

Within amagmatic portions of the East African Rift System, immature faults (Biggs et al., 2010), strong, cold intact crust (Fagereng, 2013) and low b-values recorded during seismic sequences (Gaherty et al., 2019; Lavayssière et al., 2019) are all suggestive of high differential stress in the region. Furthermore, wall-rock and gouge samples from the Thyolo fault at Kalulu do not contain significant amounts of frictionally weak, authigenic phyllosilicate minerals (Williams et al., 2019), deformation experiments on representative lithologies from the Malawi Rift indicate that they are frictionally strong (coefficient of friction, μ_s >0.55; Hellebrekers et al., 2019), and the thick (30-40 km) seismogenic crust suggests that the frictional-viscous transition does not occur at shallow depths (Craig et al., 2011; Fagereng, 2013). The Thyolo fault is, however, generally oriented parallel or subparallel to basement foliation and possibly also NW-SE striking dykes (Figure 5-6, 8c), implying that reactivation of these pre-existing structures is preferred over initiation and growth of new fault surfaces. There is no evidence that the faults host authigenic minerals and clays as described in other, long-term, frictionally weak faults described in the shallow crust elsewhere (e.g. Holdsworth, 2004; Jefferies et al., 2006).

We suggest that the foliation and dykes play an important role in controlling the geometry of the Thyolo fault in the shallow crust by providing relatively well-oriented planes for reactivation, on which the sum of cohesion and frictional resistance in the current stress field is less on the pre-existing plane than the intact rock. Although well-oriented interconnected biotite foliation may be slightly weaker than the wall-rock (Behnsen and Faulkner, 2012), such planes are not obviously controlling the fault (Figure 7,8 & 9), and a combination of greater phyllosilicate content and low cohesion, compared to the wall-rock, is likely why the foliations and dyke margins are reactivated near-surface. This is consistent with fault reactivation analysis from southern Malawi, which suggests that moderately dipping NW-SE striking incohesive surfaces will reactivate even if they are slightly oblique to the ENE-WSW to E-W trending minimum principal compressive stress (Williams et al., 2019). The Thyolo fault zone contains an incohesive damage zone and fault core (Figures 7 and 8), and we do not see fault zone fluid flow indicators in our microstructural and field observations (e.g. vein networks or fault zone alteration; Wästeby et al., 2014; Williams et al., 2017) that could result in fault cohesion recovery or the growth of frictionally weak minerals (Tenthorey and Cox, 2006; Holdsworth et al., 2011)

We also suggest that interlinked mechanisms of reactivation of pre-existing surfaces and dynamic stress reorientation along the Thyolo fault may explain why some fault sections are orientated nearly perpendicular to the strike of the main fault. The overlapping geometry between the Thyolo and Muona sections may have been established early in the growth history of the Thyolo fault by the exploitation of pre-existing NW-SE striking surfaces, on which reactivation is preferred over creating new failure surfaces in the current stress field (Williams et al., 2019). Coulomb stress changes within relay zones are known to favour the creation of zigzag fault patterns (Crider and Pollard, 1998), and coseismic Coulomb stress changes around bounding faults with large overlaps favour high angle link structures rather than oblique breached relay ramps or the creation of a fault bend (Hodge et al., 2018a). These links may have originated as transform faults, as they are better oriented for transform motion, and later reactivated as normal faults, although no evidence for transform motion is preserved. Slip on orthogonal structures may also have been favoured by the presence of Stormberg dolerite dykes striking perpendicular to the Thyolo fault (Figure 6a). Although linking segments coinciding with a pre-existing dyke have not been directly observed, the margins of dykes in swarms cutting basement terrains are commonly reactivated during later deformation events (Holdsworth et al., 2020), and dolerite dykes in South Africa are known to have increased brittle damage along the dyke-basement contact zone that reduces cohesion (Senger et al., 2015). In summary, we propose that co-seismic stress changes on overlapping faults favoured shallow activation of high-angle low-cohesion zones at the contact between the pre-existing dykes and the basement, as opposed to an oblique relay zone; in this context, linkage of the Thyolo faults proto-sections could have occurred relatively quickly.

Although the Thyolo fault surface trace follows near-surface weaknesses, this mechanism is less applicable at depths where cohesion is maintained, the relative strength differences between foliations, dykes, and intact rock are smaller, and/or confining stresses too high for frictional failure. Because variably striking normal faults at shallow depth in anisotropic crust are thought to link to and initiate from more continuous structures at depth (e.g. Graymer et al., 2007; Walker et al., 2017; Hodge et al., 2018b), these near-surface low cohesion or weaker (relative to the wall-rock) fabrics alone are not sufficient to account for the geometry of the Thyolo fault at depth. In this case, it is notable that the Thyolo fault is located at or towards the edge of the Unango Terrane. Although the exact nature and location of this boundary is uncertain, it represents a high metamorphic grade boundary at the edge of the Pan-African orogenic belts. Another regional example of these boundaries includes the Lurio Belt, which borders the Nampula Complex in NE Mozambique and is observed in outcrops of mylonitic sheared leucogneiss (Bingen et al., 2009; Macey et al., 2010). If the Unango Terrane boundary is similar to this other high metamorphic grade boundary, it could represent an existing shear zone that is viscously weak because of small grain size (Watterson, 1975; Fliervoet et al., 1997; Stenvall et al., 2019), foliation of interconnected low viscosity minerals (Handy, 1990; Montési, 2013), crystal-preferred orientations conducive to plastic flow (Poirier, 1980), or provide a competency contrast across the boundary that leads to increased stress and therefore a localisation of strain (Goodwin and Tikoff, 2002). At least some of these features apply to the quartz-feldspar-biotite gneissic foliation in the Thyolo fault footwall, and would make the foliation conducive to viscous reactivation. Consequently, we consider it likely that the Thyolo fault follows a more continuous deep-seated structure (Figure 11), possibly associated with ductile reactivation of the boundary of the Unango Terrane at mid-crustal level.

Although many faults, including the Bilila-Mtakataka fault in the Makanjira Graben, Malawi (Figure 1; Hodge et al., 2018b), show both displacement minima and geometrical changes (or structural complexity) at the same locations (Peacock and Sanderson, 1991; Dawers and Anders, 1995; Walsh et al., 2003), this is clearly not the case for the Thyolo fault (Figure 5). Dyke margins and foliation planes that shape the surface trace of the Thyolo fault have not influenced the along-strike scarp height profile (Figure 5). Instead, we suggest that if the Thyolo fault is also following a more continuous structure at depth, possibly a ductile weakness associated with the edge of the Unango Terrane, then it is the heterogeneities in this weakness that dictate where along-strike variations in fault displacement are located. We refer to this as depth-dependent reactivation.

Where depth-dependent reactivation occurs, a combination of structural controls affect the fault geometry and displacement in different ways (Phillips and McCaffrey, 2019). The Thyolo fault is an example of where the fault structure at the surface is guided by shallow pre-existing fabrics and structures, which have influenced the fault orientation, the fault core and damage zone and the relay zone evolution. In contrast, deeper reactivated structures, which we suggest may be associated with ductile reactivation of shear zones at high-grade metamorphic boundaries, can explain the slightly oblique orientation of the Thyolo fault to the regional extension direction yet apparent dip-slip kinematics (see modelling by Philippon et al., 2015; Hodge et al., 2018b; Williams et al., 2019, and observations from Phillips et al., 2016; Phillips and McCaffrey, 2019), the location of scarp height minima, and its continual reactivation under a diverse range of previous extensional directions within the Lower Shire Graben (Castaing, 1991). We acknowledge the model where the primary control on rift growth is likely to be lithospheric strength (Ebinger et al., 1991); however, while the total fault length and displacement profile may indeed reflect a thick elastic crust, the detailed surface fault geometry appears affected by a combination of shallower brittle and deeper viscous structural elements.

5.4 Comparison with other continental rifts and grabens

Many of the aspects of reactivation that we observe along the Thyolo fault resemble features observed in other parts of the active East African Rift System. Localised deformation, and fast growth and linkage of the Thyolo border fault is comparable to the Okavango rift, which is also inferred to be localised along a long-lived pre-existing crustal-scale weak zone (Kinabo et al., 2007, 2008). If local fabrics only control the shallow orientation of the fault, this also explains why individual faults in Malawi can both crosscut and follow the metamorphic foliation (Hodge et al., 2018b). Furthermore, our model explains the difference between the Lower Shire Graben, where the largest topographic relief indicates that the majority of displacement occurs on the border fault (the Thyolo fault; Figure 1), and the Zomba Graben to the north, where displacement is distributed more evenly between border and intrabasin faults (Wedmore et al., 2020). Lateral heterogeneity within the lower crust beneath the Zomba Graben has been inferred to cause this more heterogeneous strain distribution, possibly by multiple localised shear zones at depth guiding distributed deformation in the upper crust and at the surface (Wedmore et al., 2020). This is a preferred explanation for strain distribution in the Zomba Graben, as it is located *within* the Unango Terrane. In contrast, the Lower Shire Graben is located towards the edge of the terrane and hence the deformation may localise towards the terrane boundary.

The northern North Sea basin is another example of a multiphase rift where faults are hosted in crystalline basement rocks. Here, lithospheric thinning and heating, as well as stress feedbacks between growing faults, control the rift-scale localisation of strain, with pre-existing shallow brittle faults thought to have little control on reactivation (Cowie et al., 2005; Claringbould et al., 2017). Along the Thyolo fault, we have shown that shallow features affect the geometry but not the displacement profile of the fault. This is consistent with the results from the North Sea basin, suggesting that reactivation of shallow pre-existing structures and fabrics may have only a surficial role in controlling the geometry but not the accumulation of displacement of faults in rifts within crystalline, dry, continental crust. This differs from studies where a major role in rift evolution has been suggested for upper crustal faults (e.g. Bellahsen & Daniel, 2005; Duffy et al., 2015; Heilman et al., 2019; Katumwehe et al., 2015; Laõ-Dávila et al., 2015; Whipp et al., 2014). This confirms the need to consider the scale- and depth-dependence of pre-existing structures when assessing fault reactivation, where the pre-existing weaknesses may control macro- but not meso-scale structural development (Kirkpatrick et al., 2013; Samsu et al., 2020).

5.5 Implications for seismic hazard assessment

Geometrical criteria to define fault segments are commonly used to assess rupture scenarios for seismic hazard assessments (Crone and Haller, 1991a; Lettis et al., 2002; Wesnousky, 2008). We find that earthquake ruptures have persistently propagated through significant changes in fault geometry and suggest that shallow brittle structures only have a superficial, geometric effect on fault segmentation. Instead, the displacement profile may provide a better indication of fault segment boundaries controlled by a deeper, more continuous structure (Figure 11). This result differs from findings on the Wasatch fault, USA, where DuRoss et al. (2016) suggest that displacement profiles have limited value for identifying segment boundaries that restrict earthquake ruptures. Thus, our findings may only apply in regions where pre-existing fabrics play an important role in guiding the surface geometry of a fault. This presents a challenge when segmentation criteria based on shallow structures is used for assessing earthquake magnitudes for seismic hazard analyses (e.g. Field et al., 2009; Petersen et al., 2015; Valentini et al., 2019): where depth-dependent segmentation is not correctly identified, multi-segment and multi-fault ruptures such as those observed in the 2016 earthquakes in central Italy (M_w6.2, 6.1 & 6.6) and Kaikoura, New Zealand (M_w7.8) or the 2010 M_w7.2 El Mayor-Cucapah, Mexico earthquake (Wei et al., 2011; Hamling et al., 2017; Walters et al., 2018) may become more likely than is apparent from surficial indicators of fault segmentation.

6. Conclusion

The Thyolo fault is the major border fault of the Lower Shire Graben, which has experienced at least three previous phases of Phanerozoic rifting. Long sections of the fault have a NW-SE strike, but these are separated by short sections that strike NE-SW. The largest NE-SW section, the Chisumbi section, is 4.8 km long, which is normally considered long enough to define a separate fault segment that accumulates displacement differently from adjacent segments. However, the location of both the Chisumbi section and other shorter sections with a prominent change in strike do not align with two segment boundaries identified by along-strike variations in the height of the active fault scarp. We find that the fault and the pre-existing foliation are broadly parallel, whereas the strike of the short sections orientated NE-SW matches the strike of dykes emplaced during a previous period of Karoo-age rifting. Using field and microstructural observations of the Thyolo fault's footwall, we estimate that the footwall fault zone is between 15-45 m wide, considerably narrower than another example of a rift bounding fault in crystalline metamorphic basement (the Dombjerg fault, Greenland; Kristensen et al., 2016). All these observations suggest that the shallow, near-surface portions of the fault are reactivating well-oriented foliation planes and near-perpendicularly oriented dyke contacts that act as weak surfaces in the shallow crust compared to the crystalline basement. However, these shallow pre-existing structures have not affected the distribution of the most recent, near-surface displacement recorded by the scarp along the fault. Instead, we suggest that the fundamental control on the growth and displacement accumulation of this rift border fault is controlled by a broadly continuous structure at depth, which is likely to be controlled by viscous reactivation of mid-crustal ductile heterogeneities, possibly associated with the edge of the Unango Terrane.

7. Acknowledgements

This work was funded by the EPSRC project ‘Prepare’ (EP/P028233/1), funded under the Global Challenges Research Fund. We thank Kondwani Dombola for his assistance with fieldwork planning and logistics. TanDEM-X data were obtained via DLR proposal DEM_GEOL0686. We thank the editor, Eric Salomon, Bob Holdsworth and one anonymous reviewer for their detailed and constructive comments that significantly improved this manuscript. The GMT software was used for most figures in this manuscript (Wessel et al., 2013). Data that were used or generated within this manuscript, including topographic profiles, scarp height measurements and foliation measurements, have been archived in the Zenodo data repository at: https://doi.org/10.5281/zenodo.3821352

References

Behnsen, J., and Faulkner, D.R., 2012, The effect of mineralogy and effective normal stress on frictional strength of sheet silicates: Journal of Structural Geology, v. 42, p. 49–61, doi:10.1016/j.jsg.2012.06.015.

Bellahsen, N., and Daniel, J.M., 2005, Fault reactivation control on normal fault growth: An experimental study: Journal of Structural Geology, v. 27, p. 769–780, doi:10.1016/j.jsg.2004.12.003.

Biggs, J., Nissen, E., Craig, T., Jackson, J., and Robinson, D.P., 2010, Breaking up the hanging wall of a rift-border fault: The 2009 Karonga earthquakes, Malawi: Geophysical Research Letters, v. 37, p. 1–5, doi:10.1029/2010GL043179.

Bingen, B., Jacobs, J., Viola, G., Henderson, I.H.C., Skår, Ø., Boyd, R., Thomas, R.J., Solli, A., Key, R.M., and Daudi, E.X.F., 2009, Geochronology of the Precambrian crust in the Mozambique belt in NE Mozambique, and implications for Gondwana assembly: Precambrian Research, v. 170, p. 231–255, doi:10.1016/j.precamres.2009.01.005.

Bloomfield, K., 1965, The geology of the Zomba Area: Bulletin of the Geological Survey, Malawi, v. 16.

Buck, W.R., 1991, Modes of continental lithospheric extension: Journal of Geophysical Research: Solid Earth, v. 96, p. 20161–20178, doi:10.1029/91JB01485.

Caine, J.S., Evans, J.P., and Forster, C.B., 1996, Fault zone architecture and permeability structure: Geology, v. 24, p. 1025–1028, doi:10.1130/0091-7613(1996)024<1025:FZAAPS>2.3.CO;2.

Castaing, C., 1991, Post-Pan-African tectonic evolution of South Malawi in relation to the Karroo and recent East African rift systems: Tectonophysics, v. 191, p. 55–

73, doi:10.1016/0040-1951(91)90232-H.

Childs, C., Manzocchi, T., Walsh, J.J., Bonson, C.G., Nicol, A., and Schöpfer, M.P.J., 2009, A geometric model of fault zone and fault rock thickness variations: Journal of Structural Geology, v. 31, p. 117–127, doi:10.1016/j.jsg.2008.08.009.

Chisenga, C., Dulanya, Z., and Jianguo, Y., 2019, The structural re-interpretation of the Lower Shire Basin in the Southern Malawi rift using gravity data: Journal of African Earth Sciences, v. 149, p. 280–290, doi:10.1016/j.jafrearsci.2018.08.013.

Chorowicz, J., 2005, The East African rift system: Journal of African Earth Sciences, v. 43, p. 379–410, doi:10.1016/j.jafrearsci.2005.07.019.

Chorowicz, J., and Sorlien, C., 1992, Oblique extensional tectonics in the Malawi Rift, Africa: Geological Society of America Bulletin, v. 104, p. 1015–1023, doi:10.1130/0016-7606(1992)104<1015:OETITM>2.3.CO;2.

Claringbould, J.S., Bell, R.E., Jackson, C.A.L., Gawthorpe, R.L., and Odinsen, T., 2017, Pre-existing normal faults have limited control on the rift geometry of the northern North Sea: Earth and Planetary Science Letters, v. 475, p. 190–206, doi:10.1016/j.epsl.2017.07.014.

Collettini, C., and Sibson, R.H., 2001, Normal faults, normal friction? Geology, v. 29, p. 927, doi:10.1130/0091-7613(2001)029<0927:NFNF>2.0.CO;2.

Cowie, P.A., 1998, A healing-reloading feedback control on the growth rate of seismogenic faults: Journal of Structural Geology, v. 20, p. 1075–1087, doi:10.1016/S0191-8141(98)00034-0.

Cowie, P.A., and Scholz, C.H., 1992a, Displacement-length scaling relationship for faults: data synthesis and discussion: Journal of Structural Geology, v. 14, p. 1149–1156, doi:10.1016/0191-8141(92)90066-6.

Cowie, P.A., and Scholz, C.H., 1992b, Growth of faults by accumulation of seismic slip: Journal of Geophysical Research, v. 97, p. 11085, doi:10.1029/92JB00586.

Cowie, P.A., and Scholz, C.H., 1992c, Physical explanation for the displacement-length relationship of faults using a post-yield fracture mechanics model: Journal of Structural Geology, v. 14, p. 1133–1148, doi:10.1016/0191-8141(92)90065-5.

Cowie, P.A., Underhill, J.R., Behn, M.D., Lin, J., and Gill, C.E., 2005, Spatio-temporal evolution of strain accumulation derived from multi-scale observations of Late Jurassic rifting in the northern North Sea: A critical test of models for lithospheric extension: Earth and Planetary Science Letters, v. 234, p. 401–419, doi:10.1016/j.epsl.2005.01.039.

Craig, T.J., Jackson, J.A., Priestley, K., and Mckenzie, D., 2011, Earthquake distribution patterns in Africa: Their relationship to variations in lithospheric and geological structure, and their rheological implications: Geophysical Journal International, v. 185, p. 403–434, doi:10.1111/j.1365-246X.2011.04950.x.

Crider, J.G., and Pollard, D.D., 1998, Fault linkage: Three-dimensional mechanical interaction between echelon normal faults: Journal of Geophysical Research: Solid Earth, v. 103, p. 24373–24391, doi:10.1029/98jb01353.

Crone, A.J., and Haller, K.M., 1991a, Segmentation and the coseismic behavior of Basin and Range normal faults: examples from east-central Idaho and southwestern Montana, U.S.A.: Journal of Structural Geology, v. 13, p. 151–164, doi:10.1016/0191-8141(91)90063-O.

Crone, A.J., and Haller, K.M., 1991b, Segmentation and the coseismic behavior of Basin and Range normal faults: examples from east-central Idaho and southwestern Montana, U.S.A.: Journal of Structural Geology, v. 13, p. 151–164, doi:10.1016/0191-8141(91)90063-O.

Daly, M.C., Chorowicz, J., and Fairhead, J.D., 1989, Rift basin evolution in Africa: The influence of reactivated steep basement shear zones: Geological Society Special Publication, v. 44, p. 309–334, doi:10.1144/GSL.SP.1989.044.01.17.

Dawers, N.H., and Anders, M.H., 1995, Displacement-length scaling and fault linkage: Journal of Structural Geology, v. 17, p. 607–614, doi:10.1016/0191-8141(94)00091-D.

Dawers, N.H., Anders, M.H., and Scholz, C.H., 1993, Growth of normal faults: displacement-length scaling: Geology, v. 21, p. 1107–1110, doi:10.1130/0091-7613(1993)021<1107:GONFDL>2.3.CO;2.

Dixey, F., and Campbell Smith, W., 1929, The rocks of the Lupata Gorge and the north side of the lower Zambezi: Geological Magazine, v. 66, p. 241–259.

Duffy, O.B., Bell, R.E., Jackson, C.A.L., Gawthorpe, R.L., and Whipp, P.S., 2015, Fault growth and interactions in a multiphase rift fault network: Horda Platform, Norwegian North Sea: Journal of Structural Geology, v. 80, p. 99–119, doi:10.1016/j.jsg.2015.08.015.

DuRoss, C.B., Personius, S.F., Crone, A.J., Olig, S.S., Hylland, M.D., Lund, W.R., and Schwartz, D.P., 2016, Fault segmentation: New concepts from the Wasatch Fault Zone, Utah, USA: Journal of Geophysical Research: Solid Earth, v. 121, p. 1131–1157, doi:10.1002/2015JB012519.

Ebinger, C., 2005, Continental break-up: The East African perspective: Astronomy and Geophysics, v. 46, p. 2.16-2.21, doi:10.1111/j.1468-4004.2005.46216.x.

Ebinger, C.J., 1989, Geometric and kinematic development of border faults and accommodation zones, Kivu-Rusizi Rift, Africa: Tectonics, v. 8, p. 117–133, doi:10.1029/TC008i001p00117.

Ebinger, C., Djomani, Y.P., Mbede, E., Foster, A., and Dawson, J.B., 1997, Rifting

Archaean lithosphere: the Eyasi-Manyara-Natron rifts, East Africa: Journal of the Geological Society, v. 154, p. 947–960, doi:10.1144/gsjgs.154.6.0947.

Ebinger, C.J., Karner, G.D., and Weissel, J.K., 1991, Mechanical strength of extended continental lithosphere: Constraints from the Western Rift System, East Africa: Tectonics, v. 10, p. 1239–1256, doi:10.1029/91TC00579.

Eby, G.N., Roden-Tice, M., Krueger, H.L., Ewing, W., Faxon, E.H., and Woolley, A.R., 1995, Geochronology and cooling history of the northern part of the Chilwa Alkaline Province, Malawi: Journal of African Earth Sciences, v. 20, p. 275–288, doi:10.1016/0899-5362(95)00054-W.

Ekström, G., Nettles, M., and Dziewoński, A.M., 2012, The global CMT project 2004-2010: Centroid-moment tensors for 13,017 earthquakes: Physics of the Earth and Planetary Interiors, v. 200–201, p. 1–9, doi:10.1016/j.pepi.2012.04.002.

Fagereng, Å., 2013, Fault segmentation, deep rift earthquakes and crustal rheology: Insights from the 2009 Karonga sequence and seismicity in the Rukwa-Malawi rift zone: Tectonophysics, v. 601, p. 216–225, doi:10.1016/j.tecto.2013.05.012.

Field, E.H. et al., 2009, Uniform California Earthquake Rupture Forecast, Version 2 (UCERF 2): Bulletin of the Seismological Society of America, v. 99, p. 2053–2107, doi:10.1785/0120080049.

Fliervoet, T.F., White, S.H., and Drury, M.R., 1997, Evidence for dominant grain-boundary sliding deformation in greenschist- and amphibolite-grade polymineralic ultramylonites from the Redbank Deformed Zone, Central Australia: Journal of Structural Geology, v. 19, p. 1495–1520, doi:10.1016/S0191-8141(97)00076-X.

Fossen, H., and Rotevatn, A., 2016, Fault linkage and relay structures in extensional settings-A review: Earth-Science Reviews, v. 154, p. 14–28, doi:10.1016/j.earscirev.2015.11.014.

Fullgraf, T., Dombola, K., Hyvonen, E., Thomas, B., and Zammit, C. The Provisional GEMMAP 1:1 Million Scale structural and geological maps of Malawi: Geological Survey of Malawi,.

Gaherty, J.B. et al., 2019, Faulting processes during early-stage rifting: Seismic and geodetic analysis of the 2009-2010 Northern Malawi earthquake sequence: Geophysical Journal International, v. 217, p. 1767–1782, doi:10.1093/gji/ggz119.

Gawthorpe, R.L., Jackson, C.A.-L., Young, M.J., Sharp, I.R., Moustafa, A.R., and Leppard, C.W., 2003, Normal fault growth, displacement localisation and the evolution of normal fault populations: the Hammam Faraun fault block, Suez rift, Egypt: Journal of Structural Geology, v. 25, p. 883–895, doi:10.1016/S0191-8141(02)00088-3.

Gawthorpe, R.L., and Leeder, M.R., 2000, Tectono-sedimentary evolution of active extensional basins: Basin Research, v. 12, p. 195–218, doi:10.1111/j.1365-2117.2000.00121.x.

Giba, M., Walsh, J.J., and Nicol, A., 2012, Segmentation and growth of an obliquely reactivated normal fault: Journal of Structural Geology, v. 39, p. 253–267, doi:10.1016/j.jsg.2012.01.004.

Goodwin, L.B., and Tikoff, B., 2002, Competency contrast, kinematics, and the development of foliations and lineations in the crust: Journal of Structural Geology, v. 24, p. 1065–1085, doi:10.1016/S0191-8141(01)00092-X.

Graymer, R.W., Langenheim, V.E., Simpson, R.W., Jachens, R.C., and Ponce, D.A., 2007, Relatively simple through-going fault planes at large-earthquake depth may be concealed by the surface complexity of strike-slip faults: Geological

Society, London, Special Publications, v. 290, p. 189–201, doi:10.1144/SP290.5.

Gupta, A., and Scholz, C.H., 2000, A model of normal fault interaction based on observations and theory: Journal of Structural Geology, v. 22, p. 865–879, doi:10.1016/S0191-8141(00)00011-0.

Habgood, F., 1963, The geology of the country west of the Shire River between Chikwawa and Chiromo: Bulletin of the Geological Survey, Malawi, v. 14.

Habgood, F., Holt, D.N., and Walshaw, R.D., 1973, The geology of the Thyolo Area: Bulletin of the Geological Survey, Malawi, v. 22.

Hamling, I.J. et al., 2017, Complex multifault rupture during the 2016 Mw 7.8 Kaikōura earthquake, New Zealand: Science, v. 356, doi:10.1126/science.aam7194.

Handy, M.R., 1990, The solid-state flow of polymineralic rocks: Journal of Geophysical Research, v. 95, p. 8647, doi:10.1029/JB095iB06p08647.

Healy, D., Rizzo, R.E., Cornwell, D.G., Farrell, N.J.C., Watkins, H., Timms, N.E., Gomez-Rivas, E., and Smith, M., 2017, FracPaQ: A MATLAB™ toolbox for the quantification of fracture patterns: Journal of Structural Geology, v. 95, p. 1–16, doi:10.1016/j.jsg.2016.12.003.

Heermance, R., Shipton, Z.K., and Evans, J.P., 2003, Fault structure control on fault slip and ground motion during the 1999 rupture of the Chelungpu fault, Taiwan: Bulletin of the Seismological Society of America, v. 93, p. 1034–1050, doi:10.1785/0120010230.

Heilman, E., Kolawole, F., Atekwana, E.A., and Mayle, M., 2019, Controls of Basement Fabric on the Linkage of Rift Segments: Tectonics, v. 38, p. 1337–1366, doi:10.1029/2018TC005362.

Hellebrekers, N., Niemeijer, A.R., Fagereng, Å., Manda, B., and Mvula, R.L.S., 2019, Lower crustal earthquakes in the East African Rift System: Insights from frictional properties of rock samples from the Malawi rift: Tectonophysics, v. 767, p. 228167, doi:10.1016/j.tecto.2019.228167.

Henstra, G.A., Rotevatn, A., Gawthorpe, R.L., and Ravnås, R., 2015, Evolution of a major segmented normal fault during multiphase rifting: The origin of plan-view zigzag geometry: Journal of Structural Geology, v. 74, p. 45–63, doi:10.1016/j.jsg.2015.02.005.

Henza, A.A., Withjack, M.O., and Schlische, R.W., 2011, How do the properties of a pre-existing normal-fault population influence fault development during a subsequent phase of extension? Journal of Structural Geology, v. 33, p. 1312–1324, doi:10.1016/j.jsg.2011.06.010.

Hodge, M., Biggs, J., Fagereng, Å., Elliott, A., Mdala, H., and Mphepo, F., 2019, A semi-automated algorithm to quantify scarp morphology (SPARTA): Application to normal faults in southern Malawi: Solid Earth, v. 10, p. 27–57, doi:10.5194/se-10-27-2019.

Hodge, M., Biggs, J., Fagereng, Å., Mdala, H., Wedmore, L.N.J., and Williams, J.N., 2020, Evidence From High-Resolution Topography for Multiple Earthquakes on High Slip-to-Length Fault Scarps: The Bilila-Mtakataka Fault, Malawi: Tectonics, v. 39, doi:10.1029/2019TC005933.

Hodge, M., Fagereng, and Biggs, J., 2018a, The Role of Coseismic Coulomb Stress Changes in Shaping the Hard Link Between Normal Fault Segments: Journal of Geophysical Research: Solid Earth, v. 123, p. 797–814, doi:10.1002/2017JB014927.

Hodge, M., Fagereng, Biggs, J., and Mdala, H., 2018b, Controls on Early-Rift

Geometry: New Perspectives From the Bilila-Mtakataka Fault, Malawi: Geophysical Research Letters, v. 45, p. 3896–3905, doi:10.1029/2018GL077343.

Holdsworth, R.E., 2004, Weak Faults--Rotten Cores: Science, v. 303, p. 181–182, doi:10.1126/science.1092491.

Holdsworth, R.E., Butler, C.A., and Roberts, A.M., 1997, The recognition of reactivation during continental deformation: Journal of the Geological Society, v. 154, p. 73–78, doi:10.1144/gsjgs.154.1.0073.

Holdsworth, R.E., van Diggelen, E.W.E., Spiers, C.J., de Bresser, J.H.P., Walker, R.J., and Bowen, L., 2011, Fault rocks from the SAFOD core samples: Implications for weakening at shallow depths along the San Andreas Fault, California: Journal of Structural Geology, v. 33, p. 132–144, doi:10.1016/j.jsg.2010.11.010.

Holdsworth, R.E., Selby, D., Dempsey, E., Scott, L., Hardman, K., Fallick, A.E., and Bullock, R., 2020, The nature and age of Mesoproterozoic strike-slip faulting based on Re–Os geochronology of syntectonic copper mineralization, Assynt Terrane, NW Scotland: Journal of the Geological Society, p. jgs2020- 011, doi:10.1144/jgs2020-011.

Hollinsworth, A.D., Koehn, D., Dempster, T.J., and Aanyu, K., 2019, Structural controls on the interaction between basin fluids and a rift flank fault: Constraints from the Bwamba Fault, East African Rift: Journal of Structural Geology, v. 118, p. 236–249, doi:10.1016/j.jsg.2018.10.012.

Jackson, J., and Blenkinsop, T., 1993, THE Malaŵi Earthquake of March 10, 1989: DEep faulting within the East African Rift System: Tectonics, v. 12, p. 1131–1139, doi:10.1029/93TC01064.

Jefferies, S.P., Holdsworth, R.E., Shimamoto, T., Takagi, H., Lloyd, G.E., and Spiers, C.J., 2006, Origin and mechanical significance of foliated cataclastic rocks in the cores of crustal-scale faults: Examples from the Median Tectonic Line, Japan: Journal of Geophysical Research: Solid Earth, v. 111, p. n/a-n/a, doi:10.1029/2005JB004205.

Johnson, S.P., Rivers, T., and De Waele, B., 2005, A review of the Mesoproterozoic to early Palaeozoic magmatic and tectonothermal history of south–central Africa: implications for Rodinia and Gondwana: Journal of the Geological Society, v. 162, p. 433–450, doi:10.1144/0016-764904-028.

Karmakar, S., and Schenk, V., 2016, Mesoproterozoic UHT metamorphism in the Southern Irumide Belt, Chipata, Zambia: Petrology and in situ monazite dating: Precambrian Research, v. 275, p. 332–356, doi:10.1016/j.precamres.2016.01.018.

Katumwehe, A.B., Abdelsalam, M.G., and Atekwana, E.A., 2015, The role of pre-existing Precambrian structures in rift evolution: The Albertine and Rhino grabens, Uganda: Tectonophysics, v. 646, p. 117–129, doi:10.1016/j.tecto.2015.01.022.

Kim, Y.S., and Sanderson, D.J., 2005, The relationship between displacement and length of faults: A review: Earth-Science Reviews, v. 68, p. 317–334, doi:10.1016/j.earscirev.2004.06.003.

Kinabo, B.D., Atekwana, E.A., Hogan, J.P., Modisi, M.P., Wheaton, D.D., and Kampunzu, A.B., 2007, Early structural development of the Okavango rift zone, NW Botswana: Journal of African Earth Sciences, v. 48, p. 125–136, doi:10.1016/j.jafrearsci.2007.02.005.

Kinabo, B.D., Hogan, J.P., Atekwana, E.A., Abdelsalam, M.G., and Modisi, M.P., 2008, Fault growth and propagation during incipient continental rifting: Insight from a combined aeromagnetic and Shuttle Radar Topography Mission digital elevation model investigation of the Okavango Rift Zone, northwest Botswana: Tectonics, v. 27, p. 1–16, doi:10.1029/2007TC002154.

Kirkpatrick, J.D., Bezerra, F.H.R., Shipton, Z.K., Do Nascimento, A.F., Pytharouli, S.I., Lunn, R.J., and Soden, A.M., 2013, Scale-dependent influence of pre-existing basement shear zones on rift faulting: A case study from NE Brazil: Journal of the Geological Society, v. 170, p. 237–247, doi:10.1144/jgs2012-043.

Kolawole, F., Atekwana, E.A., Laó-Dávila, D.A., Abdelsalam, M.G., Chindandali, P.R., Salima, J., and Kalindekafe, L., 2018, High resolution electrical resistivity and aeromagnetic imaging reveal the causative fault of the 2009 Mw 6.0 Karonga, Malawi Earthquake: Geophysical Journal International, v. 213, p. 1–47, doi:10.1093/gji/ggy066.

Kristensen, T.B., Rotevatn, A., Peacock, D.C.P., Henstra, G.A., Midtkandal, I., and Grundvåg, S.A., 2016, Structure and flow properties of syn-rift border faults: The interplay between fault damage and fault-related chemical alteration (Dombjerg Fault, Wollaston Forland, NE Greenland): Journal of Structural Geology, v. 92, p. 99–115, doi:10.1016/j.jsg.2016.09.012.

Kröner, A., Willner, A.P., Hegner, E., Jaeckel, P., and Nemchin, A., 2001, Single zircon ages, PT evolution and Nd isotopic systematics of high-grade gneisses in southern Malawi and their bearing on the evolution of the Mozambique belt in southeastern Africa: Precambrian Research, v. 109, p. 257–291, doi:10.1016/S0301-9268(01)00150-4.

Laõ-Dávila, D.A., Al-Salmi, H.S., Abdelsalam, M.G., and Atekwana, E.A., 2015, Hierarchical segmentation of the Malawi Rift: The influence of inherited lithospheric heterogeneity and kinematics in the evolution of continental rifts: Tectonics, v. 34, p. 2399–2417, doi:10.1002/2015TC003953.

Lavayssière, A., Drooff, C., Ebinger, C., Gallacher, R., Illsley-Kemp, F., Oliva, S.J., and Keir, D., 2019, Depth Extent and Kinematics of Faulting in the Southern Tanganyika Rift, Africa: Tectonics, v. 38, p. 842–862, doi:10.1029/2018TC005379.

Leeder, M.R., and Gawthorpe, R.L., 1987, Sedimentary models for extensional tilt-block/half-graben basins: Geological Society, London, Special Publications, v. 28, p. 139–152, doi:10.1144/GSL.SP.1987.028.01.11.

Lettis, W., Bachhuber, J., Witter, R., Brankman, C., Randolph, C.E., Barka, A., Page, W.D., and Kaya, A., 2002, Influence of Releasing Step-Overs on Surface Fault Rupture and Fault Segmentation: Examples from the 17 August 1999 Izmit Earthquake on the North Anatolian Fault, Turkey: Bulletin of the Seismological Society of America, v. 92, p. 19–42, doi:10.1785/0120000808.

Macdonald, R., Crossley, R., and Waterhouse, K.S., 1983, Karroo basalts of southern Malawi and their regional petrogenetic significance: Mineralogical Magazine, v. 47, p. 281–289, doi:10.1180/minmag.1983.047.344.02.

Macey, P.H. et al., 2010, Mesoproterozoic geology of the Nampula Block, northern Mozambique: Tracing fragments of Mesoproterozoic crust in the heart of Gondwana: Precambrian Research, v. 182, p. 124–148, doi:10.1016/j.precamres.2010.07.005.

Machette, M.N., Personius, S.F., Nelson, A.R., Schwartz, D.P., and Lund, W.R., 1991, The Wasatch fault zone, utah—segmentation and history of Holocene earthquakes: Journal of Structural Geology, v. 13, p. 137–149, doi:10.1016/0191-8141(91)90062-N.

Manda, B.W.C., Cawood, P.A., Spencer, C.J., Prave, T., Robinson, R., and Roberts, N.M.W., 2019, Evolution of the Mozambique Belt in Malawi constrained by granitoid U-Pb, Sm-Nd and Lu-Hf isotopic data: Gondwana Research, v. 68, p. 93–107, doi:10.1016/j.gr.2018.11.004.

McConnell, R.B., 1967, The East African Rift System: Nature, v. 215, p. 578–581, doi:10.1038/215578a0.

McLeod, A.E., Dawers, N.H., and Underhill, J.R., 2008, The propagation and linkage of normal faults: insights from the Strathspey-Brent-Statfjord fault array, northern North Sea: Basin Research, v. 12, p. 263–284, doi:10.1111/j.1365-2117.2000.00124.x.

Mitchell, T.M., and Faulkner, D.R., 2009, The nature and origin of off-fault damage surrounding strike-slip fault zones with a wide range of displacements: A field study from the Atacama fault system, northern Chile: Journal of Structural Geology, v. 31, p. 802–816, doi:10.1016/j.jsg.2009.05.002.

Montési, L.G.J., 2013, Fabric development as the key for forming ductile shear zones and enabling plate tectonics: Journal of Structural Geology, v. 50, p. 254–266, doi:10.1016/j.jsg.2012.12.011.

Morewood, N.C., and Roberts, G.P., 2000, The geometry, kinematics and rates of deformation within an en echelon normal fault segment boundary, central Italy: Journal of Structural Geology, v. 22, p. 1027–1047, doi:10.1016/S0191-8141(00)00030-4.

Morley, C.K., 2010, Stress re-orientation along zones of weak fabrics in rifts: An explanation for pure extension in ‘oblique’ rift segments? Earth and Planetary Science Letters, v. 297, p. 667–673, doi:10.1016/j.epsl.2010.07.022.

Mortimer, E., Kirstein, L.A., Stuart, F.M., and Strecker, M.R., 2016, Spatio-temporal trends in normal-fault segmentation recorded by low-temperature thermochronology: Livingstone fault scarp, Malawi Rift, East African Rift System: Earth and Planetary Science Letters, v. 455, p. 62–72, doi:10.1016/j.epsl.2016.08.040.

Mortimer, E., Paton, D.A., Scholz, C.A., Strecker, M.R., and Blisniuk, P., 2007, Orthogonal to oblique rifting: effect of rift basin orientation in the evolution of the North basin, Malawi Rift, East Africa: Basin Research, v. 19, p. 393–407, doi:10.1111/j.1365-2117.2007.00332.x.

Muirhead, J.D., and Kattenhorn, S.A., 2018, Activation of preexisting transverse structures in an evolving magmatic rift in East Africa: Journal of Structural Geology, v. 106, p. 1–18, doi:10.1016/j.jsg.2017.11.004.

Muirhead, J.D., Wright, L.J.M., and Scholz, C.A., 2019, Rift evolution in regions of low magma input in East Africa: Earth and Planetary Science Letters, v. 506, p. 332–346, doi:10.1016/j.epsl.2018.11.004.

Nicol, A., Childs, C., Walsh, J.J., Manzocchi, T., and Schöpfer, M.P.J., 2017, Interactions and growth of faults in an outcrop-scale system: Geological Society, London, Special Publications, v. 439, p. 23–39, doi:10.1144/SP439.9.

Nicol, A., Walsh, J., Berryman, K., and Nodder, S., 2005, Growth of a normal fault by the accumulation of slip over millions of years: Journal of Structural Geology, v. 27, p. 327–342, doi:10.1016/j.jsg.2004.09.002.

Ord, D.M., Clemmey, H., and Leeder, M.R., 1988, Interaction between faulting and sedimentation during Dinantian extension of the Solway basin, SW Scotland: Journal - Geological Society (London), v. 145, p. 249–259, doi:10.1144/gsjgs.145.2.0249.

Peacock, D.C.., and Sanderson, D.., 1991, Displacements, segment linkage and relay ramps in normal fault zones: Journal of Structural Geology, v. 13, p. 721–733, doi:10.1016/0191-8141(91)90033-F.

Petersen, M.D. et al., 2015, The 2014 United States National Seismic Hazard Model: Earthquake Spectra, v. 31, p. S1–S30, doi:10.1193/120814EQS210M.

Philippon, M., Willingshofer, E., Sokoutis, D., Corti, G., Sani, F., Bonini, M., and Cloetingh, S., 2015, Slip re-orientation in oblique rifts: Geology, v. 43, p. 147–150, doi:10.1130/G36208.1.

Phillips, T.B., Jackson, C.A.L., Bell, R.E., Duffy, O.B., and Fossen, H., 2016, Reactivation of intrabasement structures during rifting: A case study from offshore southern Norway: Journal of Structural Geology, v. 91, p. 54–73, doi:10.1016/j.jsg.2016.08.008.

Phillips, T.B., and McCaffrey, K.J.W., 2019, Terrane Boundary Reactivation, Barriers to Lateral Fault Propagation and Reactivated Fabrics: Rifting Across the Median Batholith Zone, Great South Basin, New Zealand: Tectonics, v. 38, p. 4027–4053, doi:10.1029/2019TC005772.

Poirier, J.P., 1980, Shear localization and shear instability in materials in the ductile field: Journal of Structural Geology, v. 2, p. 135–142, doi:10.1016/0191-8141(80)90043-7.

Prater, W.T. et al., 2016, Strain Accomodation of Cenezoic Rifting in the Northern Margin of the Shire Graben, Southern Malawi Rift: American Geophysical Union, Fall Meeting Abstracts,.

Roberts, E.M., Stevens, N.J., O'Connor, P.M., Dirks, P.H.G.M., Gottfried, M.D., Clyde, W.C., Armstrong, R.A., Kemp, A.I.S., and Hemming, S., 2012, Initiation of the western branch of the East African Rift coeval with the eastern branch: Nature Geoscience, v. 5, p. 289–294, doi:10.1038/ngeo1432.

Robertson, E.A.M., Biggs, J., Cashman, K. V., Floyd, M.A., and Vye-Brown, C., 2016, Influence of regional tectonics and pre-existing structures on the formation of elliptical calderas in the Kenyan Rift: Geological Society Special Publication, v. 420, p. 43–67, doi:10.1144/SP420.12.

Rotevatn, A., Jackson, C.A.L., Tvedt, A.B.M., Bell, R.E., and Blækkan, I., 2019, How do normal faults grow? Journal of Structural Geology, v. 125, p. 174–184, doi:10.1016/j.jsg.2018.08.005.

Rotevatn, A., Kristensen, T.B., Ksienzyk, A.K., Wemmer, K., Henstra, G.A., Midtkandal, I., Grundvåg, S.A., and Andresen, A., 2018, Structural Inheritance and Rapid Rift-Length Establishment in a Multiphase Rift: The East Greenland Rift System and its Caledonian Orogenic Ancestry: Tectonics, v. 37, p. 1858–1875, doi:10.1029/2018TC005018.

Samsu, A., Cruden, A.R., Micklethwaite, S., Grose, L., and Vollgger, S.A., 2020, Scale matters: The influence of structural inheritance on fracture patterns: Journal of Structural Geology, v. 130, p. 103896, doi:10.1016/j.jsg.2019.103896.

Savage, H.M., and Brodsky, E.E., 2011, Collateral damage: Evolution with displacement of fracture distribution and secondary fault strands in fault damage zones: Journal of Geophysical Research, v. 116, p. B03405, doi:10.1029/2010JB007665.

Schlische, R.W., Young, S.S., Ackermann, R. V., and Gupta, A., 1996, Geometry and scaling relations of a population of very small rift-related normal faults: Geology, v. 24, p. 683–686, doi:10.1130/0091-7613(1996)024<0683:GASROA>2.3.CO;2.

Scholz, C.H., Dawers, N.H., Yu, J.Z., Anders, M.H., and Cowie, P.A., 1993, Fault growth and fault scaling laws: preliminary results: Journal of Geophysical

Research, v. 98, p. 951–961.

Segall, P., and Pollard, D.D., 1980, Mechanics of discontinuous faults: Journal of Geophysical Research: Solid Earth, v. 85, p. 4337–4350, doi:10.1029/JB085iB08p04337.

Senger, K., Buckley, S.J., Chevallier, L., Fagereng, Å., Galland, O., Kurz, T.H., Ogata, K., Planke, S., and Tveranger, J., 2015, Fracturing of doleritic intrusions and associated contact zones: Implications for fluid flow in volcanic basins: Journal of African Earth Sciences, v. 102, p. 70–85, doi:10.1016/j.jafrearsci.2014.10.019.

Shipton, Z.K., and Cowie, P.A., 2003, A conceptual model for the origin of fault damage zone structures in high-porosity sandstone: Journal of Structural Geology, v. 25, p. 333–344, doi:10.1016/S0191-8141(02)00037-8.

Smith, M., and Mosley, P., 1993, Crustal heterogeneity and basement influence on the development of the Kenya Rift, East Africa: Tectonics, v. 12, p. 591–606, doi:10.1029/92TC01710.

Stamps, D.S., Saria, E., and Kreemer, C., 2018, A Geodetic Strain Rate Model for the East African Rift System: Scientific Reports, v. 8, p. 1–8, doi:10.1038/s41598-017-19097-w.

Stenvall, C.A., Fagereng, Å., and Diener, J.F.A., 2019, Weaker Than Weakest: On the Strength of Shear Zones: Geophysical Research Letters, v. 46, p. 7404–7413, doi:10.1029/2019GL083388.

Tenthorey, E., and Cox, S.F., 2006, Cohesive strengthening of fault zones during the interseismic period: An experimental study: Journal of Geophysical Research: Solid Earth, v. 111, p. 1–14, doi:10.1029/2005JB004122.

Torabi, A., and Berg, S.S., 2011, Scaling of fault attributes: A review: Marine and

Petroleum Geology, v. 28, p. 1444–1460, doi:10.1016/j.marpetgeo.2011.04.003.

Torabi, A., Johannessen, M.U., and Ellingsen, T.S.S., 2019, Fault Core Thickness: Insights from Siliciclastic and Carbonate Rocks: Geofluids, v. 2019, p. 1–24, doi:10.1155/2019/2918673.

Tucker, G.E., McCoy, S.W., Whittaker, A.C., Roberts, G.P., Lancaster, S.T., and Phillips, R., 2011, Geomorphic significance of postglacial bedrock scarps on normal-fault footwalls: Journal of Geophysical Research: Earth Surface, v. 116, p. 1–14, doi:10.1029/2010JF001861.

Turcotte, D.L., and Schubert, G., 2002, Geodynamics: New York, Cambridge University Press, 607 p.

Valentini, A., Duross, C.B., Field, E.H., Gold, R.D., Briggs, R.W., Visini, F., and Pace, B., 2019, Relaxing Segmentation on the Wasatch Fault Zone : Impact on Seismic Hazard: v. XX, doi:10.1785/0120190088.

Walker, R.T., Wegmann, K.W., Bayasgalan, A., Carson, R.J., Elliott, J., Fox, M., Nissen, E., Sloan, R.A., Williams, J.M., and Wright, E., 2017, The Egiin Davaa prehistoric rupture, central Mongolia: a large magnitude normal faulting earthquake on a reactivated fault with little cumulative slip located in a slowly deforming intraplate setting: Geological Society, London, Special Publications, v. 432, p. 187–212, doi:10.1144/SP432.4.

Walsh, J.J., Bailey, W.R., Childs, C., Nicol, A., and Bonson, C.G., 2003, Formation of segmented normal faults: A 3-D perspective: Journal of Structural Geology, v. 25, p. 1251–1262, doi:10.1016/S0191-8141(02)00161-X.

Walsh, J.J., Nicol, A., and Childs, C., 2002, An alternative model for the growth of faults: Journal of Structural Geology, v. 24, p. 1669–1675, doi:10.1016/S0191-8141(01)00165-1.

Walters, R.J. et al., 2018, Dual control of fault intersections on stop-start rupture in the 2016 Central Italy seismic sequence: Earth and Planetary Science Letters, v. 500, p. 1–14, doi:10.1016/j.epsl.2018.07.043.

Wästeby, N., Skelton, A., Tollefsen, E., Andrén, M., Stockmann, G., Claesson Liljedahl, L., Sturkell, E., and Mörth, M., 2014, Hydrochemical monitoring, petrological observation, and geochemical modeling of fault healing after an earthquake: Journal of Geophysical Research: Solid Earth, v. 119, p. 5727–5740, doi:10.1002/2013JB010715.

Watterson, J., 1975, Mechanism for the persistence of tectonic lineaments: Nature, v. 253, p. 520–522, doi:10.1038/253520b0.

Wedmore, L.N.J., Biggs, J., Williams, J.N., Fagereng, Å., Dulanya, Z., Mphepo, F., and Mdala, H., 2020, Active Fault Scarps in Southern Malawi and Their Implications for the Distribution of Strain in Incipient Continental Rifts: Tectonics, v. 39, doi:10.1029/2019TC005834.

Wei, S. et al., 2011, Superficial simplicity of the 2010 El Mayor–Cucapah earthquake of Baja California in Mexico: Nature Geoscience, v. 4, p. 615–618, doi:10.1038/ngeo1213.

Wesnousky, S.G., 2008, Displacement and geometrical characteristics of earthquake surface ruptures: Issues and implications for seismic-hazard analysis and the process of earthquake rupture: Bulletin of the Seismological Society of America, v. 98, p. 1609–1632, doi:10.1785/0120070111.

Wesnousky, S.G., 2006, Predicting the endpoints of earthquake ruptures: Nature, v. 444, p. 358–360, doi:10.1038/nature05275.

Wessel, P., Smith, W.H.F., Scharroo, R., Luis, J., and Wobbe, F., 2013, Generic Mapping Tools: Improved Version Released: Eos, Transactions American

Geophysical Union, v. 94, p. 409–410, doi:10.1002/2013EO450001.

Westerhof, A.P., Lehtonen, M.I., Mäkitie, H., Manninen, T., Pekkala, Y., Gustafsson, B., and Tahon, A., 2008, The Tete-Chipata Belt: a new multiple terrane element from western Mozambique and southern Zambia: Geological Survey of Finland Special PAper, v. 48, p. 145–166.

Wheeler, W.H., and Karson, J.A., 1989, Structure and kinematics of the Livingstone Mountains border fault zone, Nyasa (Malawi) Rift, southwestern Tanzania: Journal of African Earth Sciences (and the Middle East), v. 8, p. 393–413, doi:10.1016/S0899-5362(89)80034-X.

Whipp, P.S., Jackson, C.A.L., Gawthorpe, R.L., Dreyer, T., and Quinn, D., 2014, Normal fault array evolution above a reactivated rift fabric; a subsurface example from the northern Horda Platform, Norwegian North Sea: Basin Research, v. 26, p. 523–549, doi:10.1111/bre.12050.

Willemse, E.J.M., 1997, Segmented normal faults: Correspondence between three-dimensional mechanical models and field data: Journal of Geophysical Research: Solid Earth, v. 102, p. 675–692, doi:10.1029/96jb01651.

Willemse, E.J.M., Pollard, D.D., and Aydin, A., 1996, Three-dimensional analyses of slip distributions on normal fault arrays with consequences for fault scaling: Journal of Structural Geology, v. 18, p. 295–309, doi:10.1016/S0191-8141(96)80051-4.

Williams, J.N., Fagereng, Å., Wedmore, L.N.J., Biggs, J., Mphepo, F., Dulanya, Z., Mdala, H., and Blenkinsop, T., 2019, How Do Variably Striking Faults Reactivate During Rifting? Insights From Southern Malawi: Geochemistry, Geophysics, Geosystems, p. 3588–3607, doi:10.1029/2019gc008219.

Williams, J.N., Toy, V.G., Smith, S.A.F., and Boulton, C., 2017, Fracturing, fluid-rock interaction and mineralisation during the seismic cycle along the Alpine Fault: Journal of Structural Geology, v. 103, p. 151–166, doi:10.1016/j.jsg.2017.09.011.

Wilson, J.., Chester, J.., and Chester, F.., 2003, Microfracture analysis of fault growth and wear processes, Punchbowl Fault, San Andreas system, California: Journal of Structural Geology, v. 25, p. 1855–1873, doi:10.1016/S0191-8141(03)00036-1.

Woolley, A.R., 1987, Lithosphere metasomatism and the petrogenesis of the Chilwa Province of alkaline igneous rocks and carbonatites, Malawi: Journal of African Earth Sciences, v. 6, p. 891–898, doi:10.1016/0899-5362(87)90048-0.

Woolley, A.R., Bevan, J.C., and Elliott, C.J., 1979, The Karroo dolerites of southern Malawi and their regional geochemical implications: Mineralogical Magazine, v. 43, p. 487–495, doi:10.1180/minmag.1979.043.328.08.

Worthington, R.P., and Walsh, J.J., 2017, Timing, growth and structure of a reactivated basin-bounding fault: Geological Society, London, Special Publications, v. 439, p. 511–531, doi:10.1144/SP439.14.

Zangerl, C., Loew, S., and Eberhardt, E., 2006, Structure, geometry and formation of brittle discontinuities in anisotropic crystalline rocks of the Central Gotthard Massif, Switzerland: Eclogae Geologicae Helvetiae, v. 99, p. 271–290, doi:10.1007/s00015-006-1190-0.

Zhang, P., Slemmons, D.B., and Mao, F., 1991, Geometric pattern, rupture termination and fault segmentation of the Dixie Valley-Pleasant Valley active normal fault system, Nevada, U.S.A.: Journal of Structural Geology, v. 13, p. 165–176, doi:10.1016/0191-8141(91)90064-P.

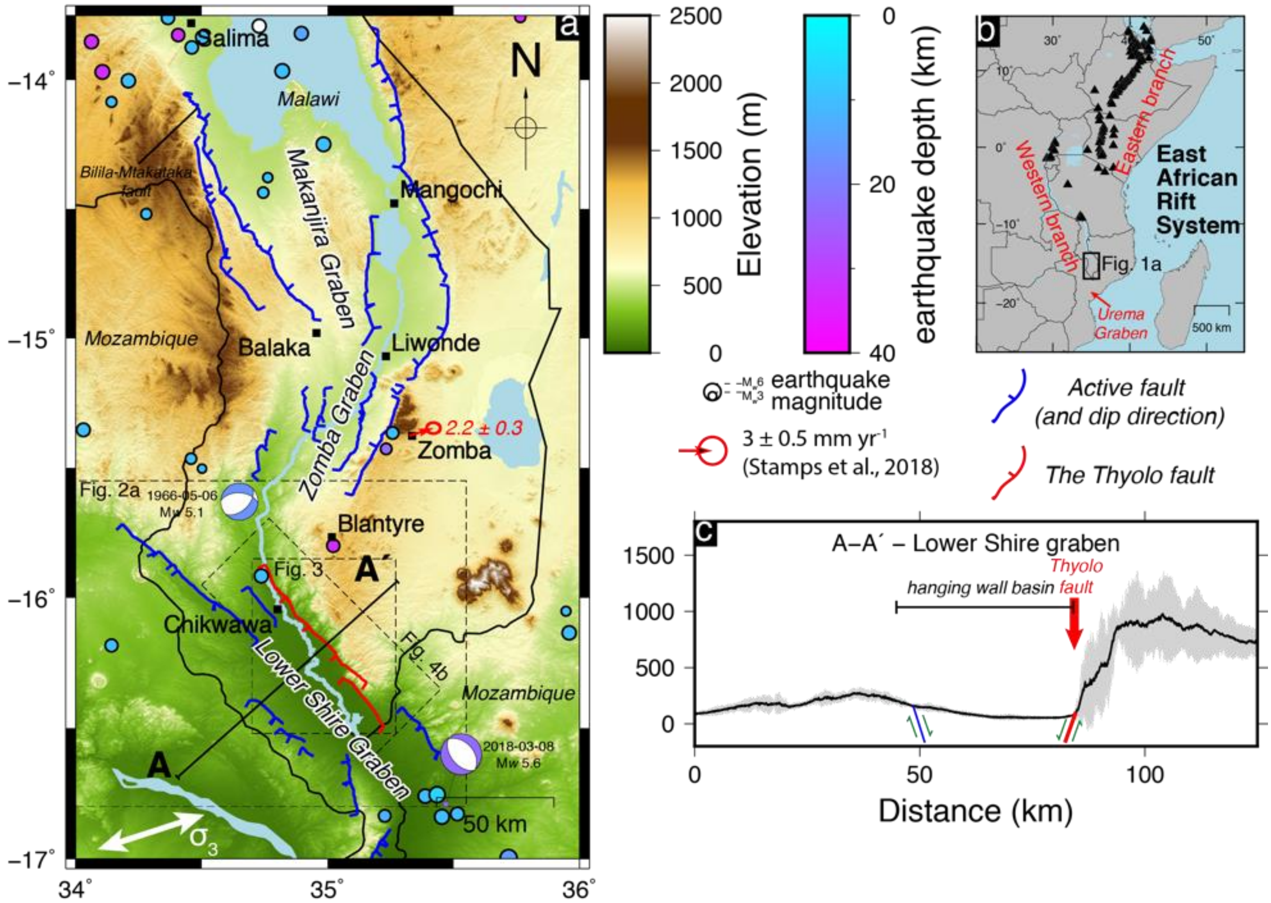

Figure 1. The location and tectonic context of the Lower Shire Graben. (a) The southern Malawi rift system with known active fault scarps in blue and the Thyolo fault highlighted in red. Also shown is the GPS vector from a station in Zomba, National Earthquake Information Centre earthquake locations from 1971-2018 (circles coloured by depth), and focal mechanisms for the two largest events in the region, a M_w5.1 earthquake in 1966 (from Craig et al., 2011) and the CMT solution for the 2018 Nsanje earthquake (M_w5.6). Extension direction (σ_3; 072°) is from a moment tensor inversion in Williams et al. (2019) (b) The location of the southern Malawi rift system within the East African Rift. Triangles indicate Holocene active volcanoes. (c) Swath topographic cross section across the Lower Shire Graben extracted from TanDEM-X data. Black line is the median elevation with the grey shading the maximum and minimum elevation 10 km either side of profile A-A` indicated in part a.

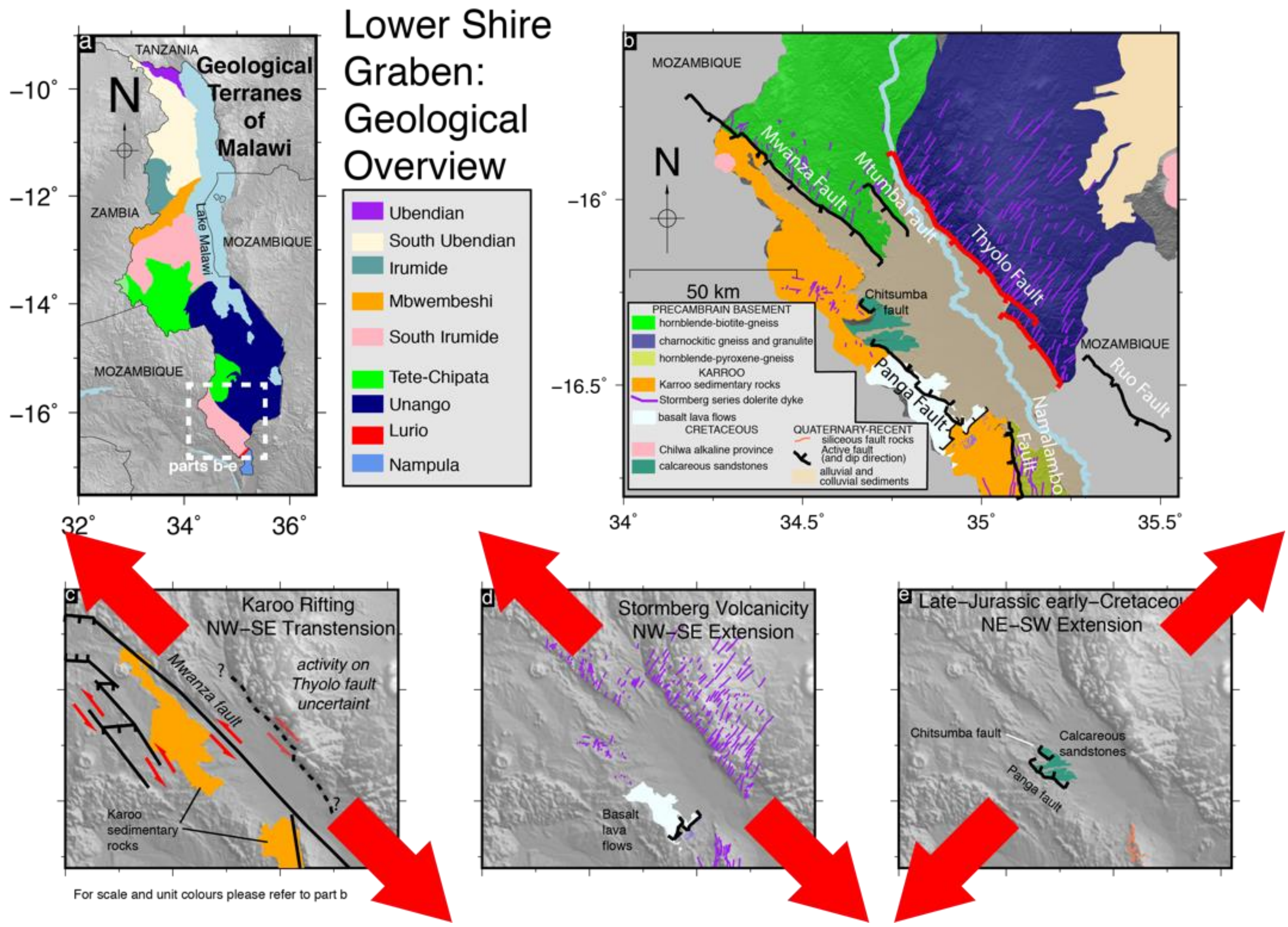

Figure 2. Geological overview of the Lower Shire Graben. (a) Geological terranes within Malawi (Fullgraf et al., *in press*). (b) Simplified geological map of the Lower Shire Graben adapted from Hapgood 1963. (c) Structures related to NW-SE Karoo-age amagmatic transtension. Note the activity of the Thyolo fault during this period is uncertain. (d) Dykes and normal faults associated with NW-SE magmatic rifting in the late Karoo period. (e) Normal faults and sedimentary deposits related to NE-SW rifting during the Late-Jurassic to early-Cretaceous.

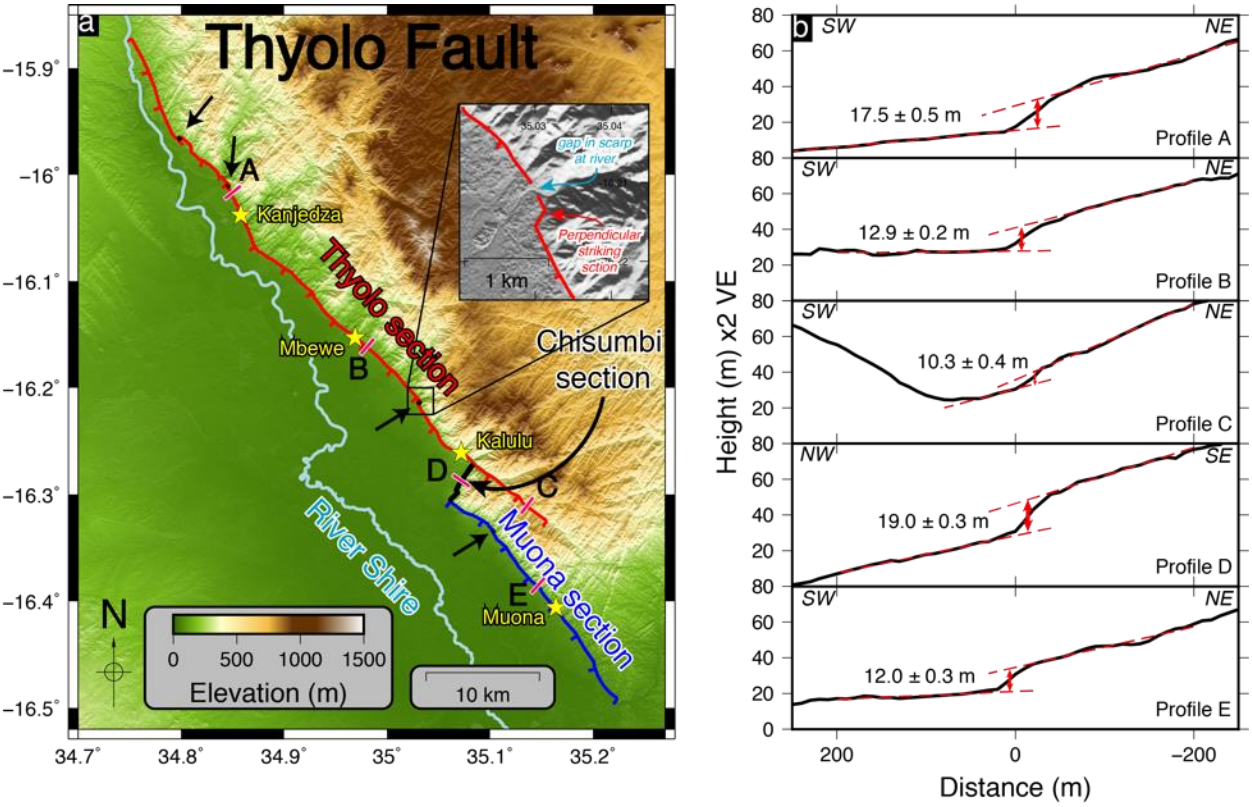

Figure 3 (a) TanDEM-X digital elevation model of the Thyolo fault showing both the Thyolo (red) and Muona (blue) sections. The fault sections oriented at ~90° to the main strike are indicated in black with sections visible at this scale identified by black arrows. Yellow stars indicate the locations of field studies reported in this paper. Pink rectangles indicate are the locations and orientation of illustrative topographic profiles extracted perpendicular to the fault scarp and shown in part b. (b) Example topographic profiles extracted perpendicular the fault scarp. All profiles are plotted with the footwall on the right-hand side (profile orientation is indicated in the top of each panel). Note profile D is located along the Chisumbi section where the strike is oriented ~90° to the strike of the main fault sections.

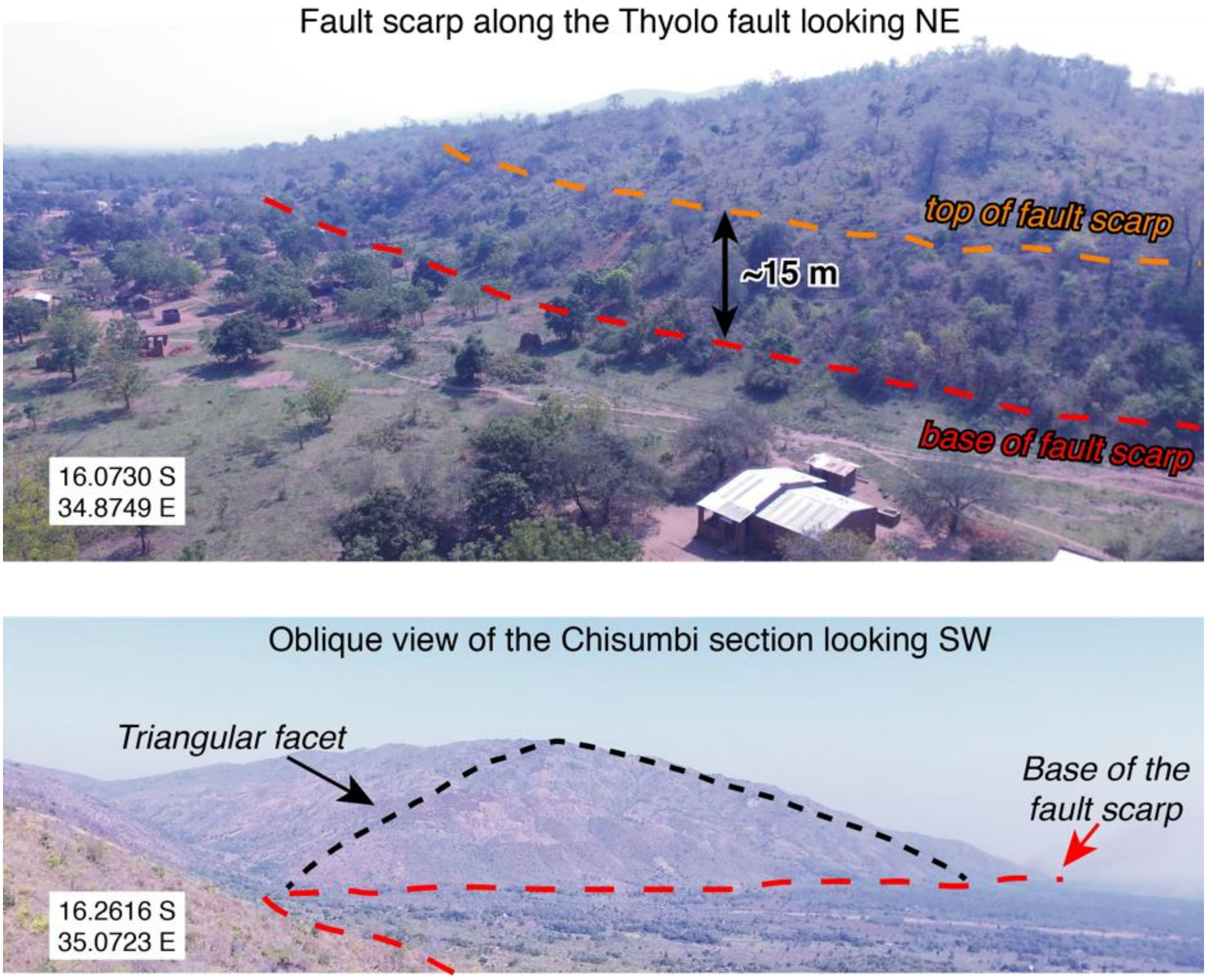

Figure 4. Field photos of the Thyolo fault. (a) An oblique view of the fault scarp along the Thyolo fault taken using a drone, showing an approximately 15 m high scarp. See the video available in the supplementary material for additional views of the scarp at this location. (b) An oblique view of the Chisumbi section taken using a drone, showing one of the triangular facets that are common along south eastern end of the fault. This section of the fault strikes perpendicular to the main section of the fault, which is just visible in the bottom left of the photo.

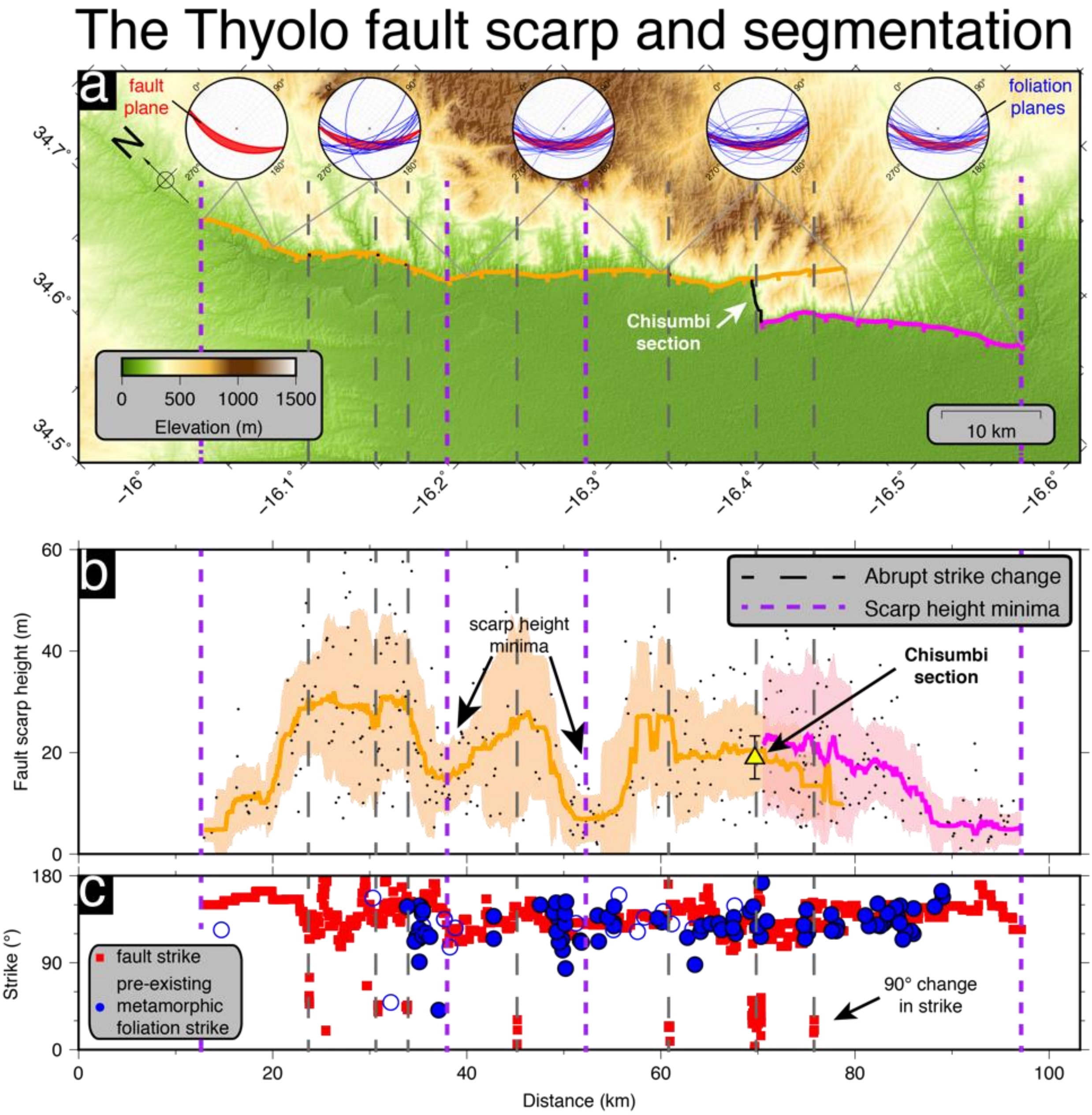

Figure 5. Thyolo fault scarp height and segmentation. (a) A rotated view of the Thyolo fault showing different indicators of fault segmentation. Inset equal angle, lower hemisphere stereonets are rotated into the same view as the underlying map. Red ellipses shows the mean fault orientation measured every 20 km, with a dip value plotted between 45°-60°, and the blue lines show foliation orientations. (b) The height of the Thyolo fault scarp as a function of distance from the NW to the SE along the fault. (c) The strike of the Thyolo fault (measured every 50 m) and foliation

strike measurements (Habgood et al., 1973) as a function of distance from NW to SE along the fault. Open blue circles represent foliation measurements that did not give details of the dip of the foliation on the original geological map (Habgood et al., 1973). Scarp height in b was measured using topographic profiles, perpendicular to the scarp, extracted every 100 m along strike. Black dots are the individual measurements with the solid coloured lines the 5 km moving median of these measurements. The shaded areas represents the 1σ error bars. Red line is the Thyolo section, blue line is the Muona section. The yellow triangle (with 1σ error bars) is the scarp height along the ~4 km linking segment.

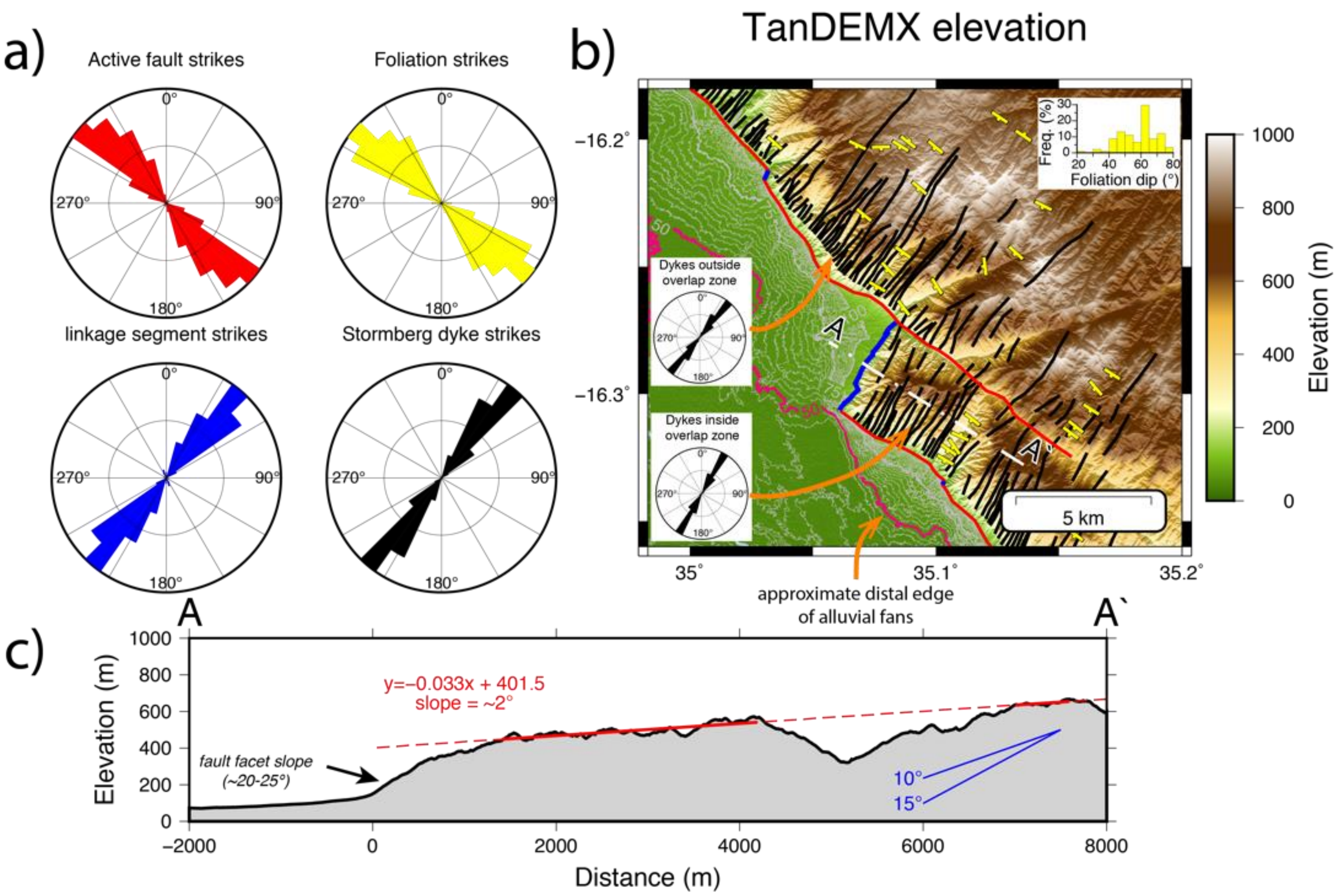

Figure 6. The Chisumbi linkage section between the Thyolo and Muona sections. (a) Rose diagrams of the orientation of surface traces of the different structures along the Thyolo fault. Active faults include the Thyolo and Muona fault sections as indicated on the map. The fault sections and dykes were divided into 50 m long sections before calculating the strike of each section. Linkage segments only include the sections of fault that strike approximately perpendicular to the Thyolo and Muona sections. Foliation orientations and Stormberg dykes were digitised from Habgood et al. (1973). (b) TanDEM-X DEM of the Chisumbi linkage section between the Thyolo and Muona sections. Dykes are indicated with black lines, foliation orientation and dip direction with yellow lines and ticks, faults with red lines and sections of the fault that strike perpendicular to the main fault with blue lines. Grey contour lines are 2.5 m apart, with the 50 m contour, which marks the approximate distal edge of alluvial fan complexes originating from footwall catchments, marked in pink. The inset

histogram shows the dip of foliation measurements (Habgood et al., 1973). The inset rose diagrams show the orientation of dykes located inside and outside of the zone where the Thyolo and Muona sections overlap. (c) Swath topographic extracted along the transect A-A` shown in part b. The mean topography 1 km either side of the transect is plotted. The red line is a linear best fit to the slope of the topography within the portions of the solid red line. The dashed portions are not used as they have been affected by erosion due to river incision or include the fault scarp and fault facet slope. Angles which are the normal range of breached relay ramp dips (according to Fossen and Rotevatn, 2016) are plotted for comparison.

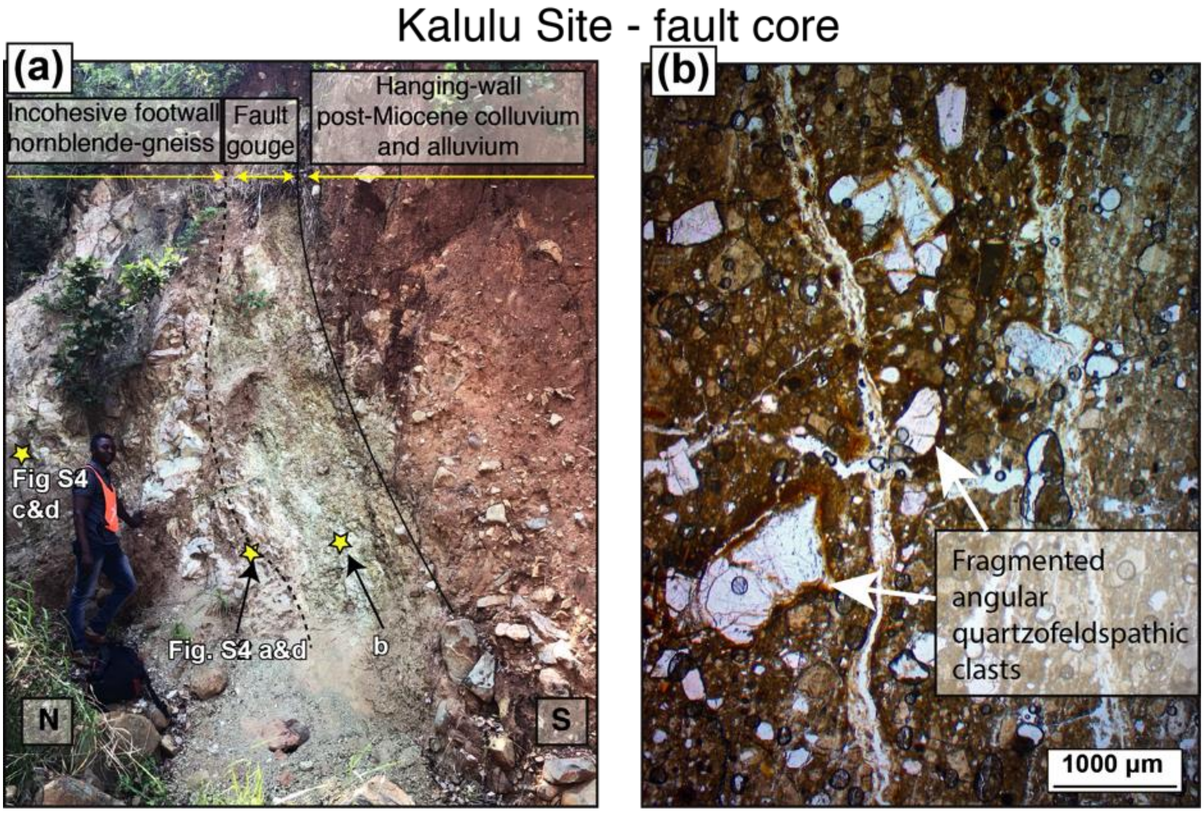

Figure 7 (a) Fault zone exposure at Kalulu showing juxtaposition of hanging wall sediments and footwall basement across a 0.7 m unit of fault gouge. Locations of samples used for photomicrographs in (b-f) shown by yellow stars. (b) photomicrograph of gouge with fractured quartz clasts and clay-rich brown matrix in plane polarised light (PPL) in sample from fault contact.

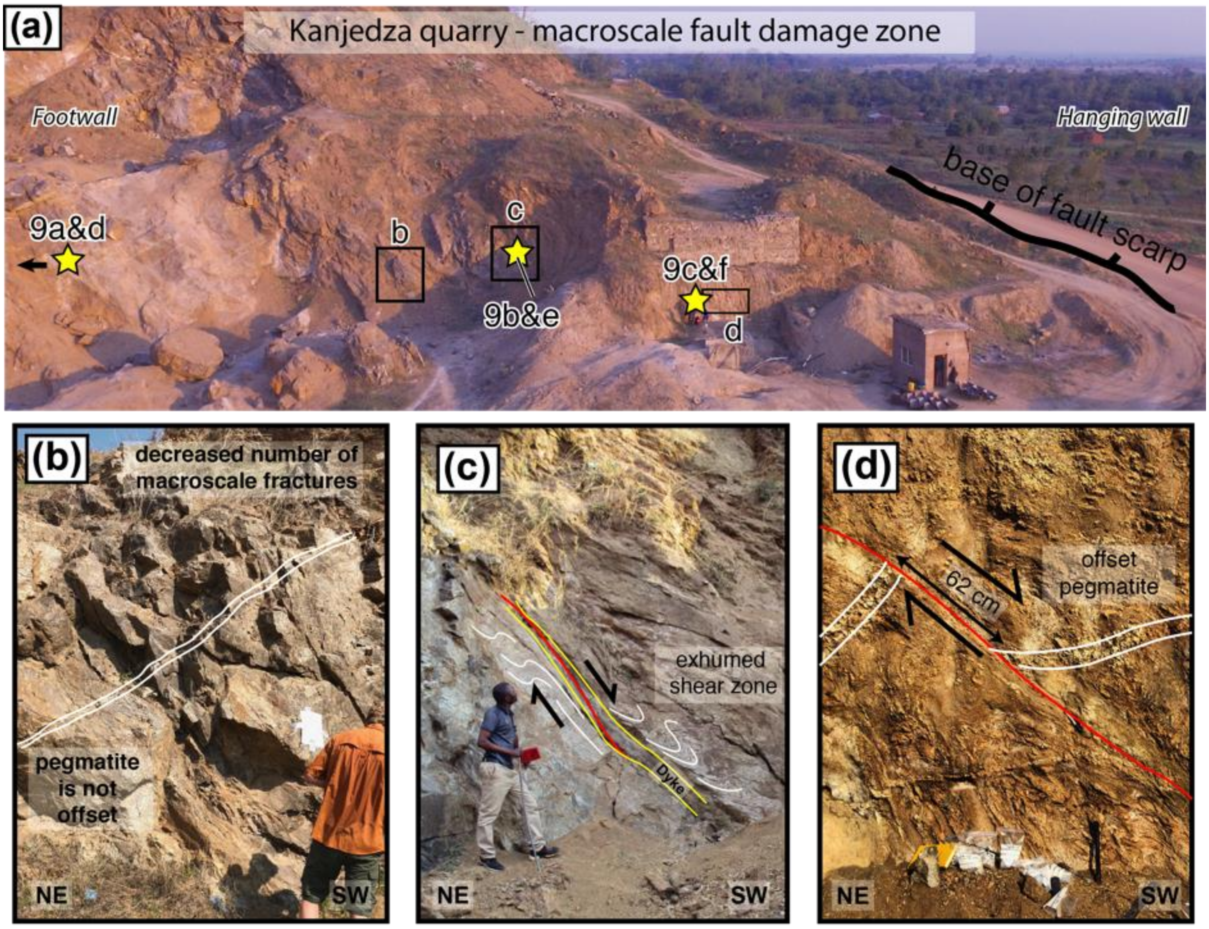

Figure 8. Macroscale fault damage zone at the Kanjedza site along the Thyolo fault. (a) A perspective view of the exposed fault zone indicating the location of sample macroscale photos shown in parts b-d. Locations of microscale observations shown in Figure 9 are indicated with yellow stars. (b) Outcrop from outside the macroscale fault damage zone, note the lack of fracturing within the basement rock when compared with c and d. (c) Outcrop within the fault damage zone showing an exhumed shear zone and dyke. We infer that the shear zone had a reverse sense of shear as we can observe the same ductile structures on both the hanging wall and footwall sides of the fault. The dyke edge has been reactivated in a normal sense and acts as a minor slip surface with the same NW-SE strike as the main fault. (d) Offset pegmatite within the footwall damage zone.

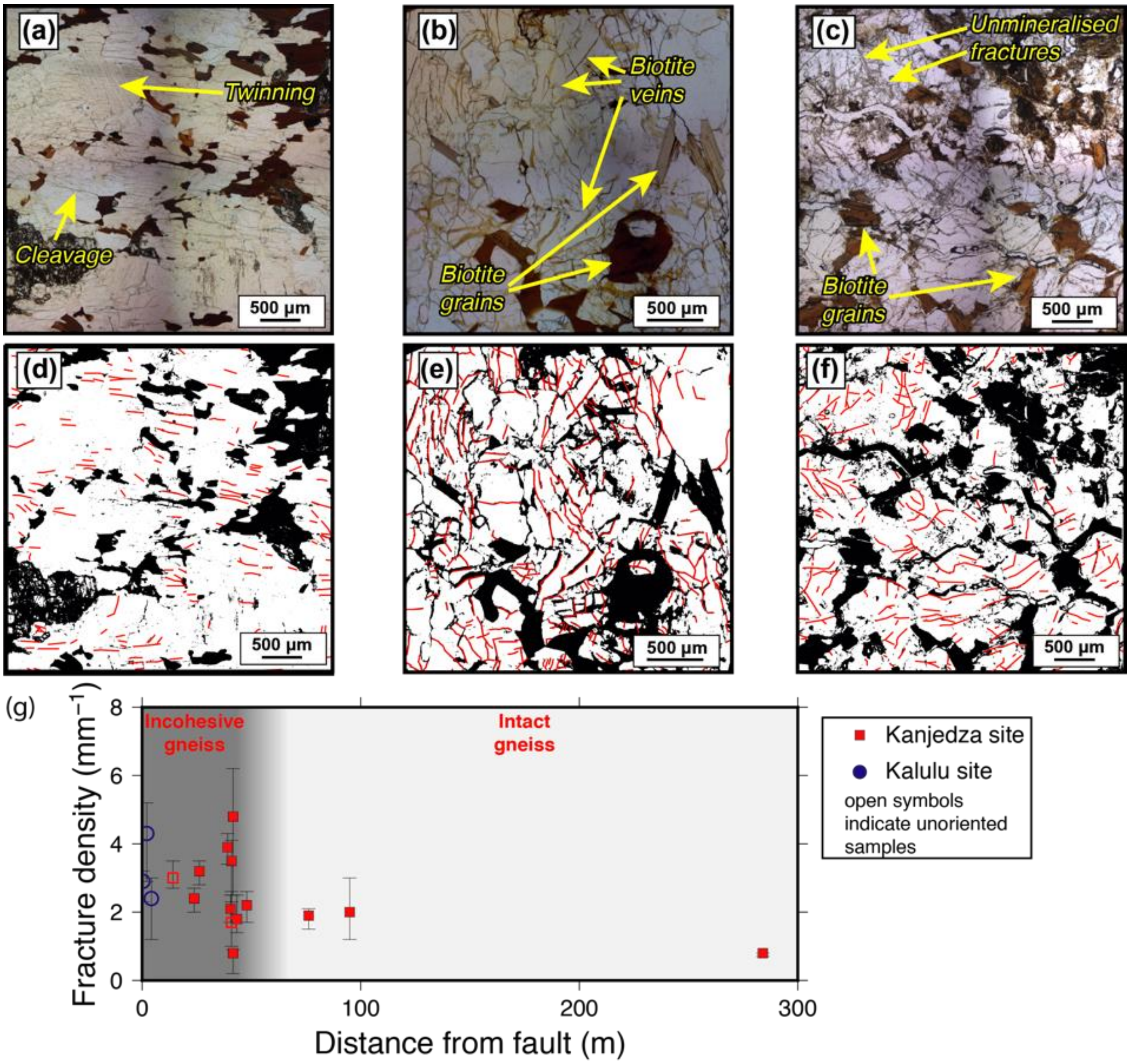

Figure 9. Microscale fault damage zone at Kanjedza Quarry. Photomicrograph of samples (a) from outside the fault zone; (b) adjacent to a minor footwall slip surface (Figure 8c); and (c) within the fault damage zone. (d-f) annotated photomicrographs of parts b-c showing the fractures (red lines) identified in each sample. (g) Compilation of fracture density plotted against distance from the fault for the Kanjedza and Kalulu sites along the Thyolo fault. The division between intact and incohesive gneiss is based on field observations (Figure 8).

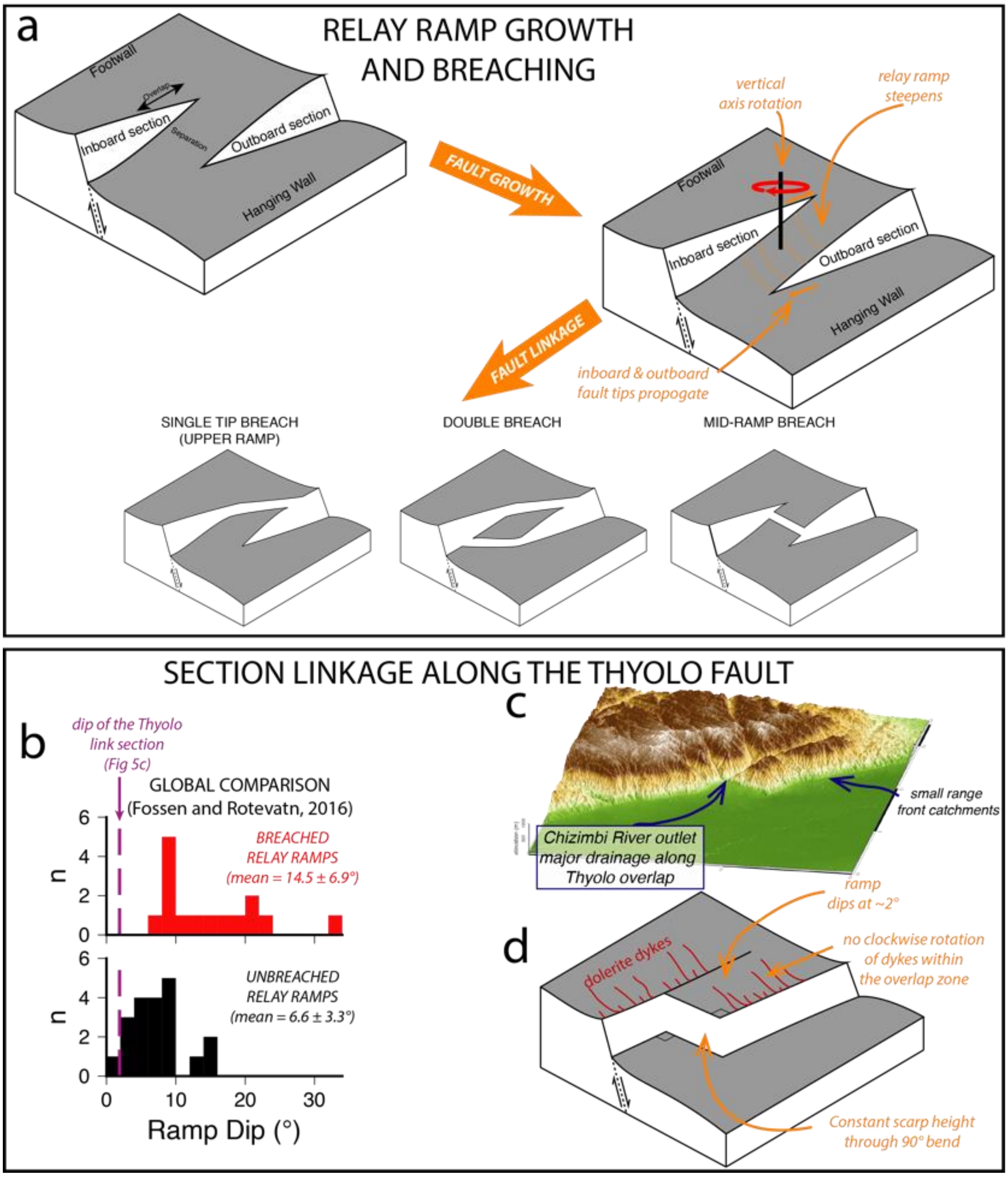

Figure 10. A comparison of relay ramp morphology and the linkage section between the Thyolo and Muona sections. (a) A summary of relay ramp growth and breaching (adapted from Fossen and Rotevatn, 2016). (b) The dip of relay ramp dips from a global compilation of breached and unbreached relay ramps (Fossen and Rotevatn, 2016). The dip of the topography in the section between the Thyolo and Muona sections is indicated with the purple dashed line. (c) A 3d view of the link section between the Thyolo and Muona sections showing the prominent drainage channels including the range front catchments that are predominate in the region and the

triangular facets along the Chisumbi section. (d) A conceptual view of the way the Thyolo fault has linked between the Thyolo and Muona sections.

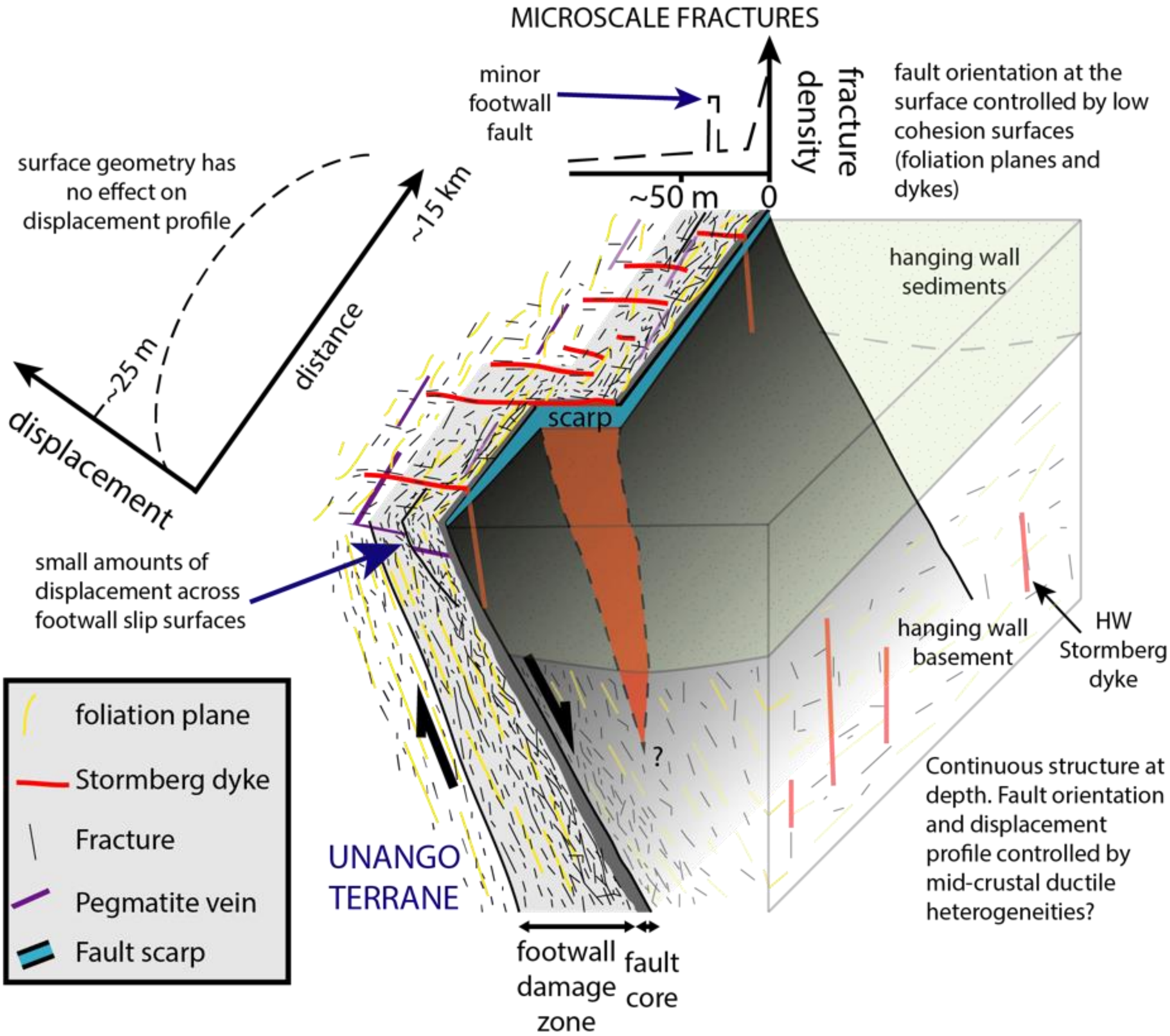

Figure 11. A conceptual model of the reactivation of the Thyolo fault towards the edge of the Unango Terrane boundary. Shallow structures, including the 90° bend and the fault damage zone are controlled by the pre-existing metamorphic foliation and dykes. In contrast, the displacement profile is not affected by these shallow structures, instead, we suggest that a deeper more continuous structure is responsible for the segmentation of the fault observed in the displacement profile. This deeper structure may be associated with the edge of the Unango Terrane.